A&A 469, 239–263 (2007)
DOI: 10.1051/0004-6361:20066772

Astronomy & Astrophysics

Evolution of asymptotic giant branch stars⋆

I. Updated synthetic TP-AGB models and their basic calibration

P. Marigo[1] and L. Girardi[2]

[1] Dipartimento di Astronomia, Università di Padova, Vicolo dell'Osservatorio 3, 35122 Padova, Italy
e-mail: paola.marigo@unipd.it
[2] Osservatorio Astronomico di Padova – INAF, Vicolo dell'Osservatorio 5, 35122 Padova, Italy
e-mail: leo.girardi@oapd.inaf.it

Received 20 November 2006 / Accepted 27 February 2007

ABSTRACT

We present new synthetic models of the TP-AGB evolution. They are computed for 7 values of initial metal content (Z from 0.0001 to 0.03) and for initial masses between 0.5 and 5.0 $M_{\odot}$, thus extending the low- and intermediate-mass tracks of Girardi et al. (2000) to the beginning of the post-AGB phase. The calculations are performed by means of a synthetic code that incorporates many recent improvements, among which we mention: (1) the use of detailed and revised analytical relations to describe the evolution of quiescent luminosity, inter-pulse period, third dredge-up, hot bottom burning, pulse cycle luminosity variations, etc.; (2) the use of variable molecular opacities – i.e. opacities consistent with the changing photospheric chemical composition – in the integration of a complete envelope model, instead of the standard choice of scaled-solar opacities; (3) the use of formalisms for the mass-loss rates derived from pulsating dust-driven wind models of C- and O-rich AGB stars; and (4) the switching of pulsation modes between the first overtone and the fundamental one along the evolution, which has consequences in terms of the history of mass loss. It follows that, in addition to the time evolution on the HR diagram, the new models also consistently predict variations in surface chemical compositions, pulsation modes and periods, and mass-loss rates. The onset and efficiency of the third dredge-up process are calibrated in order to reproduce basic observables like the carbon star luminosity functions in the Magellanic Clouds and TP-AGB lifetimes (star counts) in Magellanic Cloud clusters. In this first paper, we describe in detail the model ingredients, basic properties, and calibration. Particular emphasis is put on illustrating the effects of using variable molecular opacities. Forthcoming papers will present the theoretical isochrones and chemical yields derived from these tracks and additional tests performed with the aid of a complete population synthesis code.

Key words. stars: AGB and post-AGB – stars: carbon – stars: mass-loss – stars: general – stars: evolution – stars: abundances

1. Introduction

Owing to their high luminosities and cool photospheres, thermally pulsing asymptotic giant branch (TP-AGB) stars are among the most remarkable objects in near- and mid-infrared surveys of nearby galaxies. The TP-AGB is also one of the most intriguing phases of stellar evolution, marked by the development of high mass-loss rates, the presence of recurrent luminosity and temperature excursions, rich nucleosynthesis, and long-period variability. Several "third dredge-up" episodes – followed by hot-bottom burning (HBB) in the most massive AGB stars – cause the surface pollution with He and CNO elements of primary origin, which become directly observable first via the changes in the spectral features of AGB stars themselves, and later in the emission line spectrum of the subsequent planetary nebulae phase. In the context of galaxy models, AGB stars are crucial contributors to both their integrated spectra and their chemical enrichment.

Computations of the TP-AGB phase by means of complete evolutionary codes are very demanding in terms of computational time, and in most cases they fail to predict basic observational facts such as the conversion from M to C spectral types in AGB stars with initial masses and luminosities as low as $M_{\rm i} \sim 1.5\ M_{\odot}$ and $M_{\rm bol} \sim -3.5$ (see Herwig 2005, for a review; and Stancliffe et al. 2005, for a recent exception). Such difficulties derive from the complex structure of these stars, as well as the uncertainties in modelling convective dredge-up and mass-loss processes. In order to provide extended grids of TP-AGB models that reproduce basic observational constraints, the only viable alternative so far has been the use of the so-called synthetic codes in which the stellar evolution is described by means of simplified relations derived from complete stellar models, while convective dredge-up and mass loss are tuned by means of a few adjustable parameters.

The purpose of this paper is to describe new improved models of the TP-AGB phase of low- and intermediate mass stars, whose computation has been motivated by a series of recent improvements in the area.

1) Starting from the work by Wagenhuber & Groenewegen (1998), recent theoretical works (Karakas et al. 2002, hereafter K02; Izzard et al. 2004, hereafter I04) have significantly detailed and extended the range of validity of analytical relations describing the evolution of TP-AGB stars – e.g., the core-mass luminosity relation, inter-pulse period, pulse cycle variations, dredge-up efficiency, etc. The theoretical modelling of the mass-loss phenomenon has also significantly improved (Willson 2000; Winters et al. 2003;

⋆ Appendix A is only available in electronic form at http://www.aanda.org

Höfner et al. 2003, and references therein). Moreover, Marigo (2002) has recently demonstrated that the low-temperature opacities used in present-day TP-AGB calculations are in substantial error, due to non-consideration of the dramatic changes in molecular concentrations that occur in the outer envelope of TP-AGB stars, as their chemical composition is altered by third dredge-up episodes; the consequences of using consistent molecular opacities turn out to be remarkable when stars enter into the C-rich phase of their evolution (see Marigo 2002; Marigo et al. 2003). All these theoretical improvements should allow a better description of many aspects of the TP-AGB evolution, and also a better understanding of their dependence on the stellar mass and initial chemical composition.

2) Present-day near-infrared cameras are enormously increasing our knowledge of the AGB populations of Local Group galaxies. DENIS and 2MASS have provided photometry in the red and near-infrared for the complete sample of non-obscured AGB stars in the Magellanic Clouds, revealing striking features such as the "red tail" of carbon stars (Cioni et al. 1999; Nikolaev & Weinberg 2000). Dedicated C star surveys (e.g. Battinelli & Demers 2005a,b, and references therein), as well as future near-IR surveys using UKIRT and VISTA, will soon provide complete TP-AGB samples for a large subset of the Local Group. On the other hand, infrared surveys (IRAS, ISO, Spitzer) are revealing the samples of dust-enshrouded, optically obscured TP-AGB stars in the Magellanic Clouds (Loup et al. 1999; Cioni et al. 2003; van Loon et al. 2005; Blum et al. 2006). Interpreting these large photometric databases in terms of galaxy properties (star formation rate, age-metallicity relation, density profiles) requires the use of suitable TP-AGB models. An example of the potentialities of present-day data-sets is given by Cioni et al. (2006a,b), who detect variations in the mean stellar metallicity and star formation rate across the LMC and SMC galaxies, using only the near-IR properties of their AGB stars as compared to those predicted by theoretical models.
3) Micro-lensing surveys in the Magellanic Clouds and in the Galactic Bulge (MACHO, OGLE) have provided a huge amount of high-quality optical data for long-period variables, nicely complemented with near-IR photometry from DENIS and 2MASS. Particularly striking has been the discovery of several different sequences in the luminosity-period plan, four of which represent the various pulsation modes of AGB and upper-RGB stars (Wood et al. 1999; Soszynski et al. 2006; Groenewegen 2004; Ita et al. 2004; Fraser et al. 2005). The data clearly indicate that TP-AGB stars start pulsating as small-amplitude semi-regular variables (first and second overtones, and mixed modes) and then later in the evolution become high-amplitude Mira variables (fundamental mode). Since it is generally believed that the pulsation period correlates with the mass-loss rate of such stars, this may have important evolutionary implications that still have to be explored.

Therefore, we aim at producing TP-AGB models – and their derivatives, like isochrones, luminosity functions, synthetic colour-magnitude diagrams, etc. – including the above-mentioned improvements in the analytical relations, molecular opacities, and mass-loss prescription, and consistently predicting variations in surface chemical compositions, pulsation modes and periods, and mass-loss rates. Like in any other set of synthetic models, uncertain parameters are to be calibrated in order to reproduce basic observables, like the carbon-star luminosity functions in the Magellanic Clouds, and TP-AGB lifetimes (star counts) in star clusters. In a second phase, we intend to also check relatively new observables, like the period distributions and relative numbers of stars in the several sequences of LPVs, and the properties of dust-enshrouded AGB stars with high mass-loss.

The present paper is organised as follows. In Sect. 2 we describe model ingredients and computations. Section 3 illustrates the basic model predictions, with special emphasis put on the distinctive features found in the present calculations. Section 4, together with the Appendix, explain the calibration of model parameters, based on selected observational constraints. Finally, in Sect. 5 we briefly recall the major achievements of this work and the next steps to be followed.

2. Synthetic AGB evolution

A very detailed code for the synthetic evolution of TP-AGB stars was developed by Marigo et al. (1996, 1998) and Marigo (2001, and references therein). It couples the use of updated analytical relations (e.g., the core mass-luminosity relation, the interpulse duration) with a parametric description of the third dredge-up episodes and numerical integrations of a complete envelope model. Over the past years, several additional improvements have been introduced, the most relevant of which are briefly recalled here:

- Development of a consistent method for dealing with the over-luminosity effect caused by hydrogen burning at the bottom of the convective envelope and its related nucleosynthesis (HBB; see Marigo 1998).
- Adoption of more physically-sound dredge-up parameters, linked to the minimum post-flash temperature at the bottom of the convective envelope, $T_{\rm b}^{\rm dred}$. The two free parameters associated with the possible occurrence – described by $T_{\rm b}^{\rm dred}$ – and the efficiency – described by λ – of the third dredge-up were calibrated by fitting the carbon stars luminosity functions in both Magellanic Clouds (Marigo et al. 1999).
- Calculation of molecular opacities properly coupled to the actual chemical composition of the envelope ($\kappa_{\rm var}$), in place of the common and inappropriate choice of low-temperature opacity tables ($\kappa_{\rm fix}$) strictly valid for solar-scaled chemical mixtures (Marigo 2002; Marigo et al. 2003).

The present study stands on these previous works, adopting additional improvements to be described below. For a general description of how synthetic TP-AGB models work, the reader is referred to Groenewegen & Marigo (2003).

2.1. Initial conditions

The initial conditions at the first thermal pulse – namely total mass, luminosity, core mass, and surface chemical composition as affected by the first and second dredge-ups – are taken from Girardi et al. (2000) for the initial metallicities $Z = 0.0004$, 0.001, 0.004, 0.008, 0.019, and 0.03. For $Z = 0.0001$, we use an additional set of tracks computed by Girardi (2001, unpublished; see `http://pleiadi.oapd.inaf.it`) using the same input physics as Girardi et al. (2000). Without entering into too many details, suffice it to recall that these tracks are computed with OPAL (Iglesias & Rogers 1993, and references therein) and Alexander & Ferguson (1994) opacities and include a moderate

amount of convective core overshooting[1]. As a consequence of overshooting, the upper mass limit for the development of the AGB phase is located close to 5 $M_\odot$ (instead of the ∼8 $M_\odot$ found in classical models) for all values of Z and is slightly uncertain because the initial phase of carbon burning has not been followed in detail (see Sect. 3.1 in Girardi et al. 2000). Therefore, $M_\mathrm{i} = 5\ M_\odot$ is the highest initial mass to be considered in this work.

Finally, we note that throughout this paper, except when otherwise stated, the term initial mass is equivalent to the stellar mass at the first thermal pulse, as the pre-AGB evolution in Girardi et al. (2000) is followed at constant mass. The effect of mass loss on lower-mass models while evolving on the red giant branch (RGB) will be considered a posteriori in the construction of stellar isochrones (Marigo & Girardi, in prep.).

2.2. Luminosity and core-mass growth

Important improvements have been introduced into the present calculations to follow (i) the evolution of the stellar luminosity $L(t)$ and, (ii) the growth rate of the core mass $\mathrm{d}M_\mathrm{c}/\mathrm{d}t = L_\mathrm{H}\ Q_\mathrm{H}/X(\mathrm{H})$, where L_H is the rate of energy generation due to radiative shell H-burning, Q_H is the emitted energy per unit mass of H burnt into He, and $X(\mathrm{H})$ is the H abundance in the stellar envelope.

To this aim we first need to choose a core mass-luminosity ($M_\mathrm{c} - L$) relation, among the various ones available in the literature. This key-ingredient of any synthetic AGB model is usually derived from complete AGB evolutionary calculations by fitting the surface luminosity at the stage of the quiescent preflash maximum as a function of the core mass, and possibly including the effect of other less influential parameters (metallicity, envelope mass, initial conditions at the first thermal pulse).

For lower-mass models not experiencing HBB, we adopt the core mass-luminosity ($M_\mathrm{c} - L$) relationship provided by Wagenhuber & Groenewegen (1988; their Eq. (5)), which includes important effects like dependence on metallicity and the peculiar behaviour due to the first thermal pulses.

The deviation from the $M_\mathrm{c} - L$ relation due to the overluminosity produced by HBB in more massive models (i.e. with $M_\mathrm{i} > 3.5$–$4.5\ M_\odot$, depending on metallicity) is estimated as an additional term according to I04 (their Eq. (32)). This correction depends on metallicity and takes the increase in the core degeneracy during the TP-AGB evolution into account. This means that, even when M_c remains almost constant in massive AGB stars with very deep dredge-up ($\lambda \approx 1$), the surface luminosity still increases because of the increasing core degeneracy.

It is important to notice that the $M_\mathrm{c} - L$ relation is strictly valid under the quiescent conditions just before a thermal pulse, while significant deviations (i.e. the so-called rapid dip, rapid peak and slow dip) take place during the interpulse period due to the complex interplay between the occurrence of the flash and the consequent structural and thermal readjustment across the star. Compared to our previous studies – where a very simplified description of the rapid peak and slow dip was adopted – a crucial implementation in our synthetic code is that, with the aid of the formalism proposed by Wagenhuber & Groenewegen (1988), we now follow the evolution in detail of both $L(t)$ and $L_\mathrm{H}(t)$, which vary significantly during thermal pulse cycles.

[1] Namely, in these models the overshooting parameter Λ_c (see Alongi et al. 1993) is set to 0.5 for initial masses $M_I \geq 1.5\ M_\odot$, which implies an overshooting region extending for about 0.25 pressure scale heights *above* the classical Schwarzschild border. For $M_I < 1.5\ M_\odot$, Λ_c is gradually reduced until it becomes null for $M_I \leq 1.0\ M_\odot$.

Figures 1 and 2 provide examples of the detailed description of the luminosity variations driven by thermal pulses (left panels) and the evolution of the core mass (right panels) in models of different masses and metallicities. These results closely agree with full calculations of the TP-AGB phase (see e.g., Figs. 4–9 in Vassiliadis & Wood 1993). We note that, except for the final stages of intense mass loss, the most massive models ($M_\mathrm{i} = 4\ M_\odot$) do not show the rapid luminosity peaks because of their high envelope mass and that they are also affected by HBB while evolving in luminosity well above the $M_\mathrm{c} - L$ relation.

It is worth noting that the growth of the core mass due to shell H-burning during the inter-pulses period may be followed by a quasi-instantaneous reduction due to convective dredge-up at thermal pulses. Such recursive increase-recession of the core mass creates the saw-like behaviour displayed by all models in the righthand panels of Figs. 1 and 2 (except for the 1.0 $M_\odot$, $Z = 0.008$ case which does not present dredge-up). It is already clear from these figures that convective dredge-up is predicted to be more efficient in models of higher mass and lower metallicity.

Table 1 presents a few relevant quantities predicted by four test synthetic TP-AGB calculations (A-B-C-D models) for $M_\mathrm{i} = 1.8\ M_\odot$, $Z = 0.008$, carried out under various physical assumptions, namely: detailed description of the luminosity evolution ($L(t)$) or use of the quiescent core mass-luminosity relation ($M_\mathrm{c} - L$ rel.); adoption of molecular opacities for solar-scaled chemical mixtures (κ_fix) or coupled with the current envelope composition (κ_var); inclusion or not of the third dredge-up. The other table entries correspond to predicted stellar lifetimes covering the whole TP-AGB phase ($\tau_\mathrm{TP-AGB}$), the M-type phase (τ_M) with C/O<1 and $\log L/L_\odot > 3.3$, the C-type phase (τ_C) with C/O>1; final stellar mass (M_f) and surface C/O ratio; effective temperature at the onset of the superwind regime of mass loss ($T_\mathrm{eff}(\dot{M}_\mathrm{SW})$). Model A corresponds to our reference case, obtained with the "best" combination of physical assumptions at our disposal. It turns out that the results obtained by simply assuming the $M_\mathrm{c} - L$ relation over the entire interpulse period (model B) are quite different from those found with a more realistic description of the pulse cycle (model A). In fact, even though both calculations end up with almost the same final mass, the duration of the whole TP-AGB evolution, as well as the M- and C-type phases are significantly shorter in model B (by ≈30–40%) than in model A. Model C, in which the third dredge-up is suppressed, predicts a sizeable reduction of the TP-AGB lifetime as well, while the C-type phase is completely missed. This simple experiment tells us that, for instance, the predicted counts of TP-AGB stars in a galaxy via a population-synthesis scheme may be affected by a substantial error if the underlying TP-AGB tracks are computed using a simplified description of the luminosity evolution, i.e. if the $M_\mathrm{c} - L$ relation is assumed anytime.

2.3. Interpulse period

The interpulse period τ_ip marks the pace of thermal pulses during the TP-AGB phase, hence affecting both the evolution over the quiescent regime (e.g., core mass and luminosity increase) and the events associated to the occurrence of He-flashes (e.g., frequency of dredge-up episodes).

In the present calculations we adopt the formalism suggested by I04, which is a modified version of the Wagenhuber & Groenewegen (1988) core mass–interpulse period relation that accounts for the increase in τ_ip seen in the more massive models with deep dredge-up. The I04 (their Eq. (28)) improvement consists in adding a positive term, depending on the

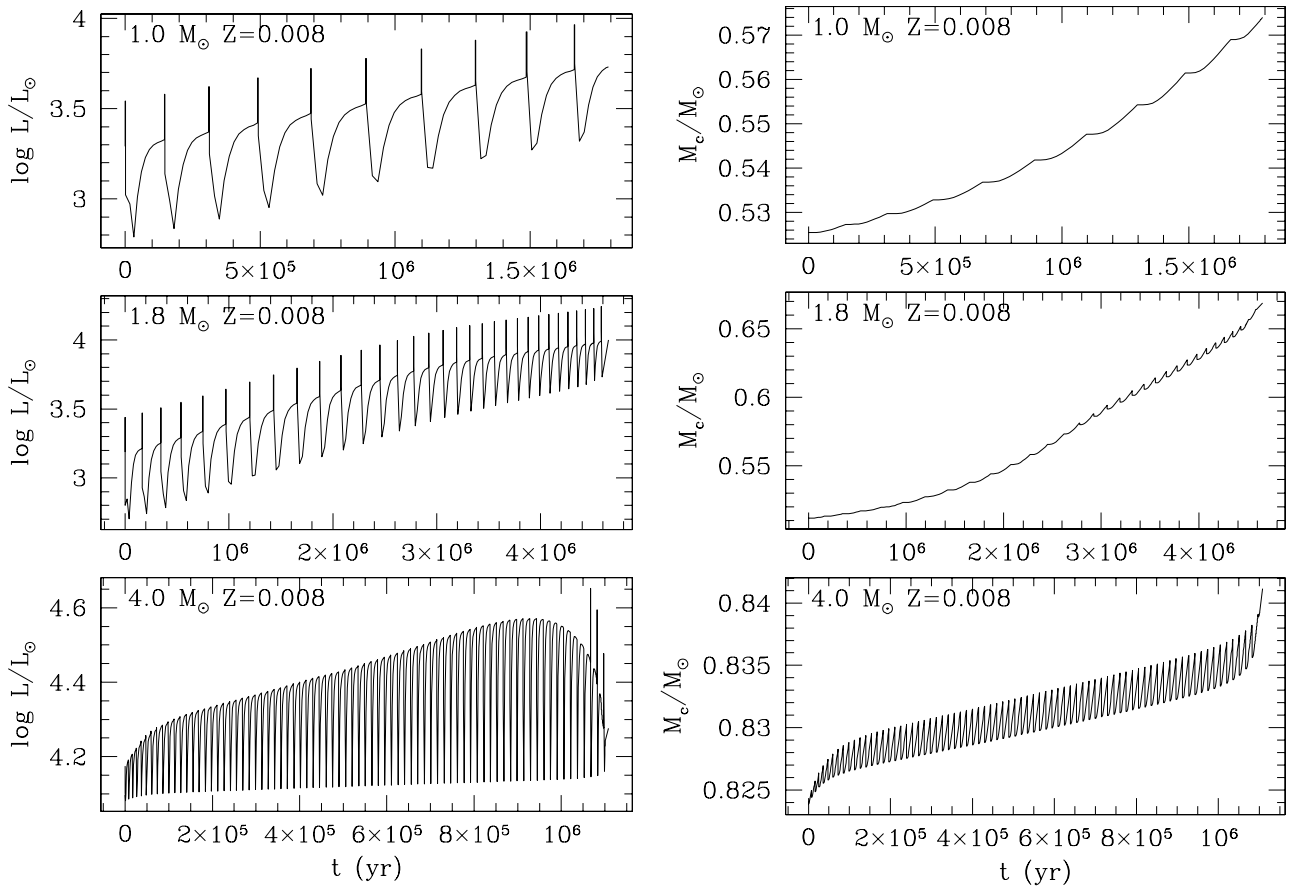

Fig. 1. *Left panels*: evolution of surface luminosity along the TP-AGB phase of two representative models with different initial masses with $Z = 0.008$, according to the analytic formalism by Wagenhuber & Groenewegen (1998). Note the high detail in the description of the luminosity variations driven by thermal pulses (i.e. peaks and dips), as well as of the overluminosity caused by the occurrence of HBB in the $4.0\,M_{\odot}$ model. *Right panels*: evolution of the core mass. The saw-like trend reflects the occurrence of dredge-up events at thermal pulses. Note that the $4.0\,M_{\odot}$ model is characterised by very deep dredge-up for most of its evolution ($\lambda \approx 1$).

dredge-up efficiency λ, to the Wagenhuber & Groenewegen's relation.

2.4. Effective temperature

The effective temperature of our TP-AGB models is derived with the aid of complete integrations of static envelope models, extending from the photosphere down to the core. The adopted integration scheme is fully described in Marigo et al. (1996, 1998, 1999) and Marigo (2002), to which the reader should refer for all details. The fundamental output of the envelope integrations is the effective temperature, which affects the properties of the TP-AGB evolution, like the position in the HR diagram, mass-loss efficiency, pulsation, colours, etc.

One crucial aspect to be noticed regards the radiative opacities at low temperatures (i.e. $T < 10\,000$ K), which are predominantly due to the molecules (and dust grains for $T < 1500$ K) that form in the coolest photospheric layers of AGB stars. Important is that we abandon the improper choice – still commonly used in evolutionary calculations of the AGB phase – of opacity tables for solar-scaled chemical composition ($\kappa_{\rm fix}$). The present TP-AGB models are computed with the adoption of the routine developed by Marigo (2002), which calculates the low-temperature molecular opacities consistently coupled with the current chemical composition of the gas ($\kappa_{\rm var}$). In this way we are able to account for the drastic opacity changes that take place as soon as a model passes from an oxygen-rich (C/O < 1) to a carbon-rich (C/O > 1) surface composition as a consequence of the third dredge-up, or when the reverse transition possibly occurs due to HBB.

Figures 3 and 4 display the evolution of the effective temperature and surface C/O ratio during the whole TP-AGB evolution of a few selected synthetic models with varying initial mass and metallicity. Thermal pulses cause the quasi-periodic complex behaviour of $T_{\rm eff}$ that essentially mirrors that of L, shown in the corresponding Figs. 1 and 2. As mentioned, the introduction of variable molecular opacities is responsible for the sudden change in the average slope of the $\log T_{\rm eff}(t)$ curve as the photospheric C/O rises above unity in models where the third dredge-up takes place. In contrast, models without the third dredge-up (e.g., $M_{\rm i} = 1.0\,M_{\odot}, Z = 0.008$) are characterised by a steady decrease in $T_{\rm eff}$ for most of their evolution (but for the latest stages of heavy mass loss). An interesting case is shown by the $M_{\rm i} = 4.0\,M_{\odot}, Z = 0.008$ model experiencing the sequence C/O $< 1 \longrightarrow$ C/O $> 1 \longrightarrow$ C/O < 1 as a consequence of the competition between the third dredge-up and HBB. Note the kind of valley in the $T_{\rm eff}$ curve specularly corresponding to the part of the C/O curve above unity.

As already demonstrated in Marigo (2002) and Marigo et al. (2003), adopting chemically-variable molecular opacities radically improves the treatment of carbon-star evolutionary

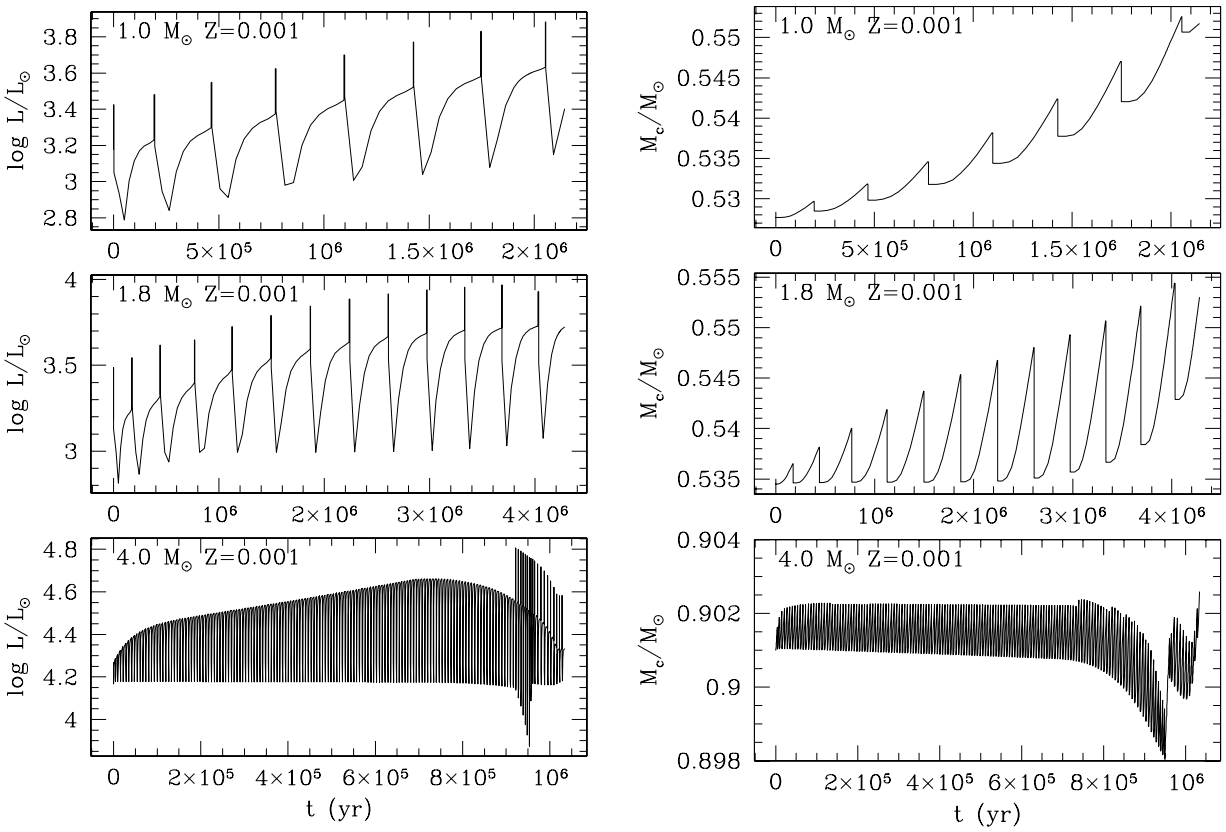

Fig. 2. The same as in Fig. 1, but for initial metallicity $Z = 0.001$.

Table 1. Predicted properties of synthetic TP-AGB models with $M_i = 1.8\ M_\odot$, $Z = 0.008$.

Model	Luminosity	Molecular opacity	3rd dredge-up	$\tau_{\rm TP-AGB}$ (Myr)	$\tau_{\rm M}$ (Myr)	$\tau_{\rm C}$ (Myr)	$M_{\rm f}$ ($M_\odot$)	$({\rm C/O})_{\rm f}$	$T_{\rm eff}(\dot{M}_{\rm SW})$ (K)
A	$L(t)$	$\kappa_{\rm var}$	yes	4.65	2.98	1.33	0.67	3.04	2630
B	$M_{\rm c} - L$ rel.	$\kappa_{\rm var}$	yes	3.09	1.85	0.89	0.66	2.84	2630
C	$M_{\rm c} - L$ rel.	$\kappa_{\rm fix}$	no	3.18	2.83	0	0.73	0.34	3311
D	$L(t)$	$\kappa_{\rm fix}$	yes	5.91	2.96	2.62	0.76	5.79	3162

models, leading to solutions of several long-lasting discrepancies between theory and observations. For instance, the red tail drawn by field carbon stars in near-infrared colour–colour diagrams of the Magellanic Clouds (e.g., DENIS, 2MASS surveys) is reproduced, as well as the low C/O and $T_{\rm eff}$ values typically found in Galactic AGB C-type stars.

In fact, the reproduction of these basic properties of C stars is not possible when using molecular opacities de-coupled from the actual surface chemical composition of C-rich models, which is still a common choice in published TP-AGB evolutionary calculations. The sharp dichotomy between the two cases ($\kappa_{\rm fix}$ and $\kappa_{\rm var}$) is exemplified in Fig. 5, which compares the predicted behaviour of $T_{\rm eff}$ in an $M_i = 1.8, Z = 0.008$ TP-AGB model with chemically-variable (model A with $\kappa_{\rm var}$ in Table 1) and with fixed, solar-scaled (model D with $\kappa_{\rm fix}$ in Table 1) molecular opacities. It is very evident that the $T_{\rm eff}$ evolution of the $\kappa_{\rm fix}$ model is not influenced at all by the behaviour of the C/O ratio, while in the $\kappa_{\rm var}$ case the rate of $T_{\rm eff}$ decrease with time speeds up significantly as the star enters the C-rich domain. As a consequence, keeping the other input prescriptions the same, the duration of the TP-AGB phase turns out shorter in the $\kappa_{\rm var}$ model compared to the $\kappa_{\rm fix}$ one.

Indeed, molecular opacities heavily affect the structure of the star's surface layers, as illustrated in Fig. 6. The significant differences between $\kappa_{\rm fix}$ and $\kappa_{\rm var}$ (top panel) strongly influence the temperature (middle panel) and density (bottom panel) stratification in the external regions. In the outermost layers, in particular (with mass coordinate $0.998 \lesssim M(r)/M \leq 1$), $\kappa_{\rm var}$ overcomes $\kappa_{\rm fix}$, which determines a sizeable reduction in the effective temperature, passing from $T_{\rm eff} \sim 3281\ K$ for $\kappa_{\rm fix}$ to $T_{\rm eff} \sim 2729\ K$ for $\kappa_{\rm var}$. As a further consequence, the $\kappa_{\rm var}$ model corresponds to a more expanded photosphere (i.e. R is forced to increase to allow the model radiate the same L), hence to lower densities (bottom panel).

At this point it is important to analyse how much such behaviour is sensitive to the metallicity. Considering that the formation of molecules in the atmospheres of AGB stars becomes less efficient at lower Z – because of the higher temperatures and the lower abundances of the involved isotopes – it follows that the cooling effect on the atmospheres of carbon stars due to molecular opacities should be less and less evident at decreasing metallicity. To give an example, by comparing Figs. 3 and 4 one already notices that the sudden change in the mean slope of the effective temperature curve, at the transition to the

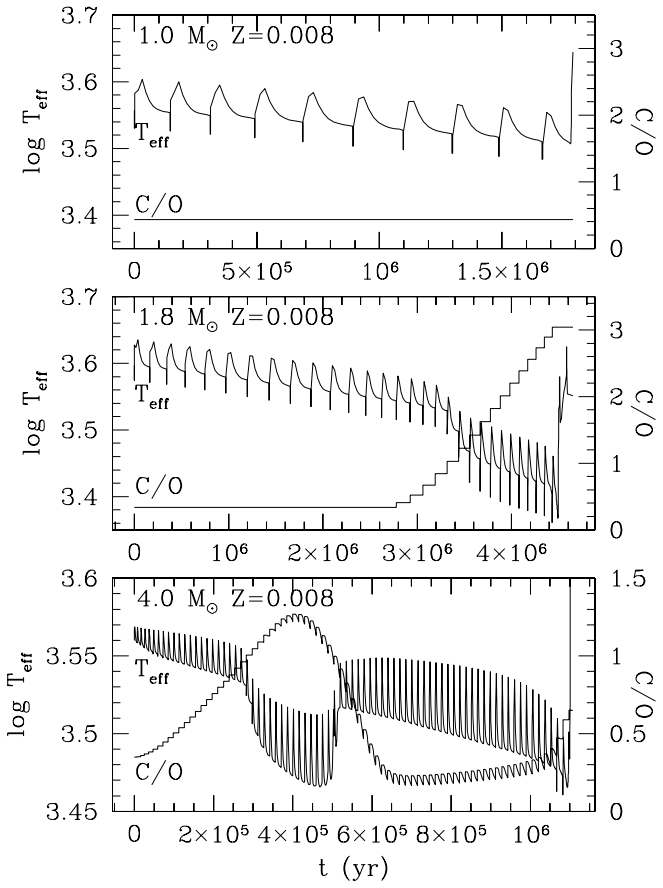

Fig. 3. Evolution of effective temperature and photosperic C/O ratio for the same models as in Fig. 1. Note the specular behaviour compared to that of the luminosity, and the remarkable average decrease in $T_{\rm eff}$ as soon as C/O increases from below to above unity. The reverse trend, i.e. an increase in $T_{\rm eff}$, occurs instead in the $4.0\,M_{\odot}$ model due to the subsequent reconversion from C/O > 1 to C/O < 1 caused by HBB.

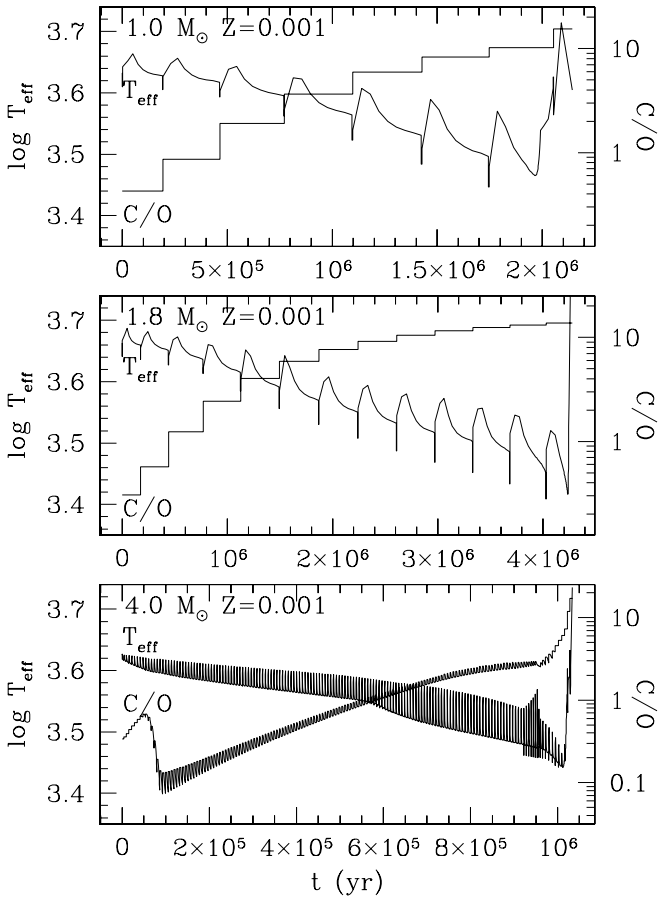

Fig. 4. The same as in Fig. 3, but for initial metallicity $Z = 0.001$.

C-star domain, is much more pronounced in TP-AGB models with $Z = 0.008$ compared to those with $Z = 0.001$. This point is better illustrated with the help of Fig. 7, which shows how the effective temperature of a selected model (with given total mass, core mass, and luminosity) is expected to behave at increasing C/O over a wide range of initial metallicities. As already mentioned, the sudden and extended excursion toward lower effective temperature as soon as C/O $\gtrsim$ 1, characterising models of higher Z, is progressively reduced at decreasing metallicity, eventually disappearing for $Z < 0.0004$.

2.5. The third dredge-up

The treatment of the third dredge-up is essentially the same one as in Marigo et al. (1999) to which the reader should refer for all details. In practice we need to specify three quantities, namely: (i) the minimum temperature at the base of the convective envelope at the stage of the post-flash luminosity maximum, $T_{\rm b}^{\rm dred}$, or equivalently the minimum core mass required for the occurrence of the mixing event, $M_{\rm c}^{\rm min}$; (ii) the efficiency of the third dredge-up λ; and (iii) the chemical composition of the intershell. Compared to our previous models (e.g., Marigo & Girardi 2001, and references therein), in this work we improve the description of the third dredge-up, thanks to the recent results of detailed calculations of the AGB phase, namely K02 and I04. The main points are summarised as follows.

2.5.1. Occurrence of dredge-up

In Marigo et al. (1999) the adopted criterion assumes that $T_{\rm b}^{\rm dred}$, derived from numerical integrations of static envelope models, is constant regardless of stellar mass and metallicity, following the indications from full AGB calculations as reported by Wood (1981). The calibration of the parameter from the fits to the observed CSLFs in the Magellanic Clouds yields $\log T_{\rm b}^{\rm dred} = 6.4$.

In this study we explore an alternative approach to $\log T_{\rm b}^{\rm dred}$ by introducing the quantity $M_{\rm c}^{\rm min}$, which is the minimum core mass required for dredge-up to take place. This has been a commonly used parameter in synthetic AGB models over the years, often assumed to be the same ($\sim 0.58\,M_{\odot}$) for any stellar mass and metallicity (Groenewegen & de Jong 1993; Marigo et al. 1996; Mouhcine & Lançon 2002). Only very recently extended grids of complete AGB models have become available (e.g., K02; I04), allowing us to relax the crude simplification of constant $M_{\rm c}^{\rm min}$ in place of a more physically sound dependence on stellar mass and metallicity.

In the present study we adopt the relations $M_{\rm c}^{\rm min}(M, Z)$, proposed by K02, based on grids of complete AGB calculations covering initial masses $M_{\rm i} = 1{-}6\,M_{\odot}$ and metallicities $Z = 0.02, 0.008, 0.004$. A partial modification of their analytical fits turns out to be necessary for the following reasons.

Systematic shift. The reproduction of the observed CSLFs in the Magellanic Clouds requires that $M_{\rm c}^{\rm min}$ is lower than predicted (Sect. 4.1; see also K02 and I04). Our synthetic calculations

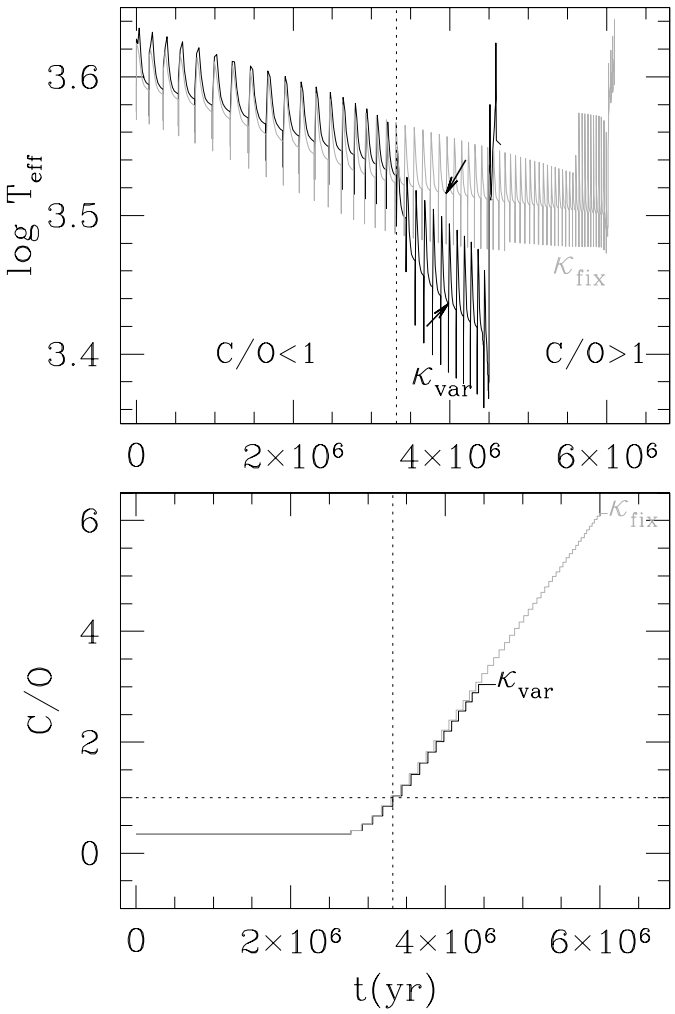

Fig. 5. Predicted behaviour of the effective temperature (*top panel*) and photospheric C/O ratio (*bottom panel*) over the entire TP-AGB evolution of a model with $M_\mathrm{i} = 1.8\,M_\odot$, $Z = 0.008$, adopting either fixed solar-scaled (model A in Table 1; gray line) or variable (model D in Table 1; black line) molecular opacities. The two T_eff curves suddenly separate as soon as the models become carbon-rich as a consequence of the third dredge-up. Arrows indicate the quiescent stage just preceeding the 24th thermal pulse in both models, whose photospheric structures are shown in Fig. 6.

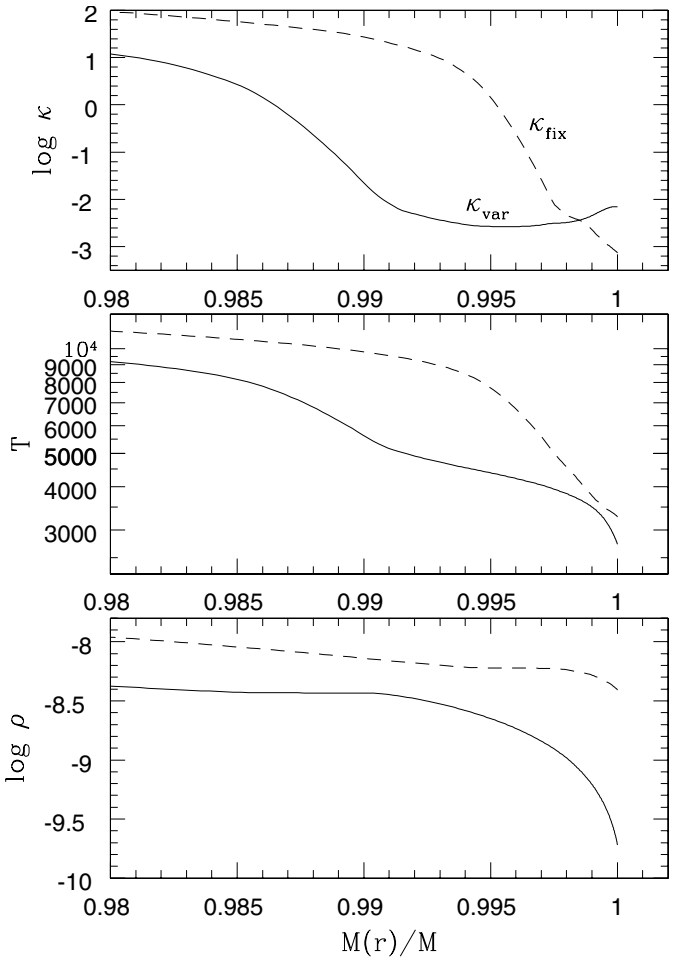

Fig. 6. Structure of the surface layers of a model with $M = 1.776\,M_\odot$, $M_\mathrm{c} = 0.632\,M_\odot$, $\log L = 3.926\,L_\odot$, and C/O = 2.560, as a function of the mass coordinate $M(r)/M$, where $M(r)$ is the mass within a sphere of radius r. From top to bottom panels we compare the behaviour of the Rosseland mean opacity ($\mathrm{cm^2\,gr^{-1}}$), the temperature, and the density (in $\mathrm{g\,cm^{-3}}$) for κ_fix (solid line) and κ_var (dashed line) cases.

indicate that $M_\mathrm{c}^\mathrm{min}$ – as given by Eq. (10) in K02 – must be decreased by an amount $\Delta M_\mathrm{c}^\mathrm{min}$ that depends on metallicity:

$$\Delta M_\mathrm{c}^\mathrm{min}/M_\odot = \max[0.1, 0.1{-}100\,(Z - 0.008)]. \quad (1)$$

The negative correction, $-\Delta M_\mathrm{c}^\mathrm{min}$, becomes larger at decreasing metallicity, e.g., $(-0.01, -0.05, -0.08)\,M_\odot$ for $Z = (0.008, 0.004, 0.001)$, respectively. This implies that for $Z \leq 0.001$ the onset of the third dredge-up in stellar models of any mass would take place since the first thermal pulse.

In practice, we limit this metallicity extrapolation imposing that no dredge-up can occur for initial masses $M < 1\,M_\odot$, in order to comply with the observed lack of intrinsic C-stars (not related to binary evolution like the CH stars or dwarf carbon stars) in Galactic globular clusters.

Correction for overshooting As far the evolution prior to the AGB is concerned, K02 do not assume overshoot from convective cores during H-burning, while a moderate convective overshoot is included in the Girardi et al. (2000) sets of tracks, from which we extract the initial conditions of our AGB models.

One important effect due to convective overshoot is that of lowering the critical mass M_HeF, which is the maximum initial stellar mass required to ignite core He-burning in degenerate conditions. At any given metallicity this limit mass is well-defined by the minimum in the relation between the core mass at the first thermal pulse, M_c^1, and the initial stellar mass M_i (see e.g., Marigo et al. 1999; K02). A similar behaviour is shared by the corresponding $M_\mathrm{c}^\mathrm{min}$ vs. M_i relation (see e.g., K02), so that the minimum of $M_\mathrm{c}^\mathrm{min}$ corresponds to M_HeF.

It follows that the inclusion of convective overshoot in stellar evolutionary calculations causes, among other effects, a decrease in M_HeF, hence a shift of the minimum $M_\mathrm{c}^\mathrm{min}(M_\mathrm{i})$ towards lower masses. In other words, the inclusion of convective overshooting can be approximately described by considering that a star with initial mass M_i behaves like a star of higher mass $f_\mathrm{ov}\,M_\mathrm{i}$ (with $f_\mathrm{ov} > 1$) without overshooting.

From a comparison between K02 and Girardi et al. (2000) models, the enhancement factor is estimated as $f_\mathrm{ov} \sim 1.2$. Hence, in order to mimic the effect of convective overshoot on the

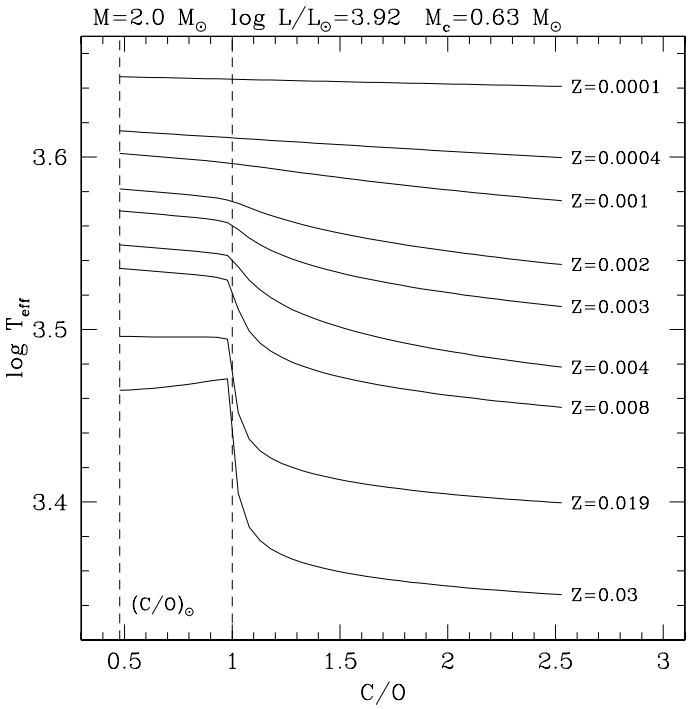

Fig. 7. Metallicity dependence of the relationship between the effective temperature and the photosphetic C/O ratio. The curves are obtained by means of envelope integrations assuming the same set of stellar input parameters (i.e. total mass, core mass, luminosity), while varying the initial metallicity, as indicated. Starting from solar C/O, the carbon abundance is progressively increased to mimic the effect of the third dredge-up. We notice that the sudden photosperic cooling caused by molecular opacities as soon as C/O > 1 is quite pronounced at higher metallicities, while it almost disappears for $Z < 0.0004$.

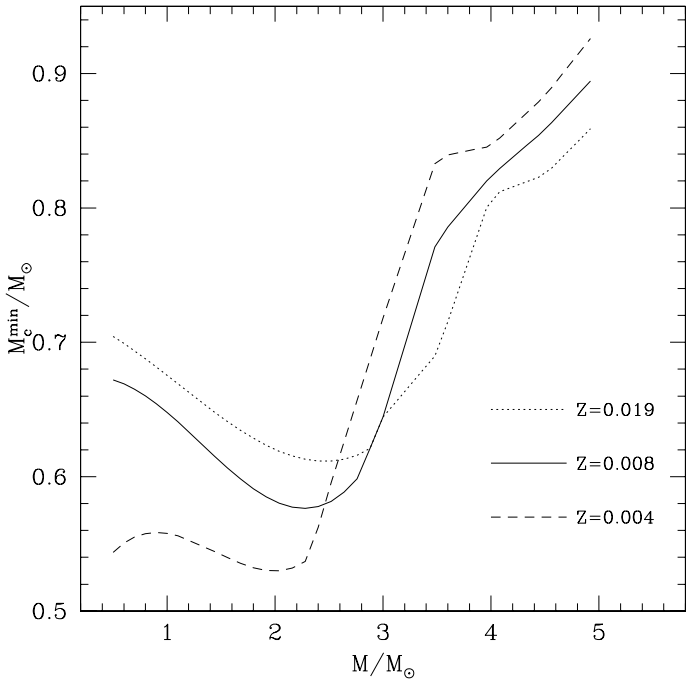

Fig. 8. Minimum core mass required for the occurrence of the third dredge-up as a function of the stellar mass at the first thermal pulse, for three choices of the initial chemical composition. In all curves the minimum corresponds to the critical mass $M_{\rm HeF}$.

relation $M_{\rm c}^{\rm min}(M_{\rm i})$, we simply adopt the K02 formalism as a function of the adjusted mass variable $\hat{M} = f_{\rm ov}\, M$:

$$M_{\rm c}^{\rm min}(M) = \left[M_{\rm c}^{\rm min}(\hat{M})\right]_{\rm K02}. \quad (2)$$

The resulting $M_{\rm c}^{\rm min}$ at varying initial stellar mass are shown in Fig. 8 for $Z = 0.019, 0.008, 0.004$. For metallicities outside the range covered by K02 models, we linearly extrapolate in Z the coefficients of the fitting polynomial functions of K02. It should be recalled that for models with initial mass $M_{\rm i} \gtrsim 3\,M_{\odot}$ the core mass predicted by Eq. (2) is lower than the core mass at the first thermal pulse $M_{\rm c,\,1TP}$, so that in these cases we set $M_{\rm c}^{\rm min} = M_{\rm c,\,1TP}$.

2.5.2. Dredge-up efficiency

We briefly recall that the efficiency of each dredge-up event is usually expressed via the quantity $\lambda = \Delta M_{\rm dred}/\Delta M_{\rm c}$, i.e. the mass brought up to the surface at a thermal pulse, $\Delta M_{\rm dred}$, normalised to the core mass increment over the preceeding interpulse period, $\Delta M_{\rm c}$.

The usual choice in previous studies has been to adopt the same λ for any value of the stellar mass. The past calibration of this parameter through the reproduction of the observed CSLFs in the Magellanic Clouds (see e.g., Marigo et al. 1999) yields $\lambda = 0.5$ for $Z = 0.008$ and $\lambda = 0.65$ for $Z = 0.004$.

In the present study we relax the assumption of constant λ, accounting for both the mass and metallicity dependences found on the base of K02 and I04 complete AGB models. In summary, once $M_{\rm c}$ has grown above $M_{\rm c}^{\rm min}$, the efficiency λ progressively increases towards an asymptotic value $\lambda_{\rm max}$, with an e-folding interval of $N_{\rm r}$ thermal pulses. This behaviour is conveniently described by the relation

$$\lambda(N) = \lambda_{\rm max}\left[1 - \exp(N/N_{\rm r})\right] \quad (3)$$

where N is the progressive pulse number ($N = 0$ as long as $M_{\rm c} < M_{\rm c}^{\rm min}$).

We use the analytical fits by K02 for $\lambda_{\rm max}$. We notice that at any given metallicity the asymptotic quantity increases with the stellar mass, typically reaching values 0.8–1.0 for $M_{\rm i} > 3\,M_{\odot}$. The metallicity dependence is weaker, such that at given stellar mass $\lambda_{\rm max}$ tends to be somewhat higher at decreasing Z.

In order to have significantly larger efficiencies at metallicities $Z < 0.004$ – that is, below the low end of the metallicity range covered by K02 models – we modify the original $\lambda_{\rm max}(M, Z)$ relation in K02 by applying a positive shift to the mass variable

$$\lambda_{\rm max}(M) = \lambda_{\rm max}(M + \Delta M_{\lambda}) \quad (4)$$

where

$$\Delta M_{\lambda} = 200\,(0.004 - Z)\,M_{\odot}. \quad (5)$$

This correction is consistent with the theoretical expectation that the third dredge-up is more efficient at lower metallicities (see Sect. 3.4 in I04 for a similar adjustment), and it is also required to reproduce the faint wing of the CSLF in the SMC, which is populated mainly by lower-mass stars with metallicities down to $\simeq$0.001 (see Sect. 4).

As discussed by K02, there is no simple law able to fit $N_{\rm r}$ as a function of M and Z. A rather satisfactory reproduction of the results for $N_{\rm r}$ presented by K02 (in their Table 5) is obtained with the function

$$N_{\rm r} = a_1 + a_2\,\left[a_3 - \exp(a_4 M_{\rm 1TP})\right] \times \left[a_5 + a_6\,\exp(a_7 - M_{\rm 1TP})^2\right]. \quad (6)$$

Table 2. Coefficients for Eq. (6).

	Z		
	0.019	0.008	0.004
a_1	4.110	2.785	2.555
a_2	42.612	10.625	809.426
a_3	5.834E-03	4.806E-02	3.348E-05
a_4	–2.113	–0.908	–4.417
a_5	2.014	0.806	1.751
a_6	–9.116	–6.708	–70.624
a_7	3.830	3.462	3.516

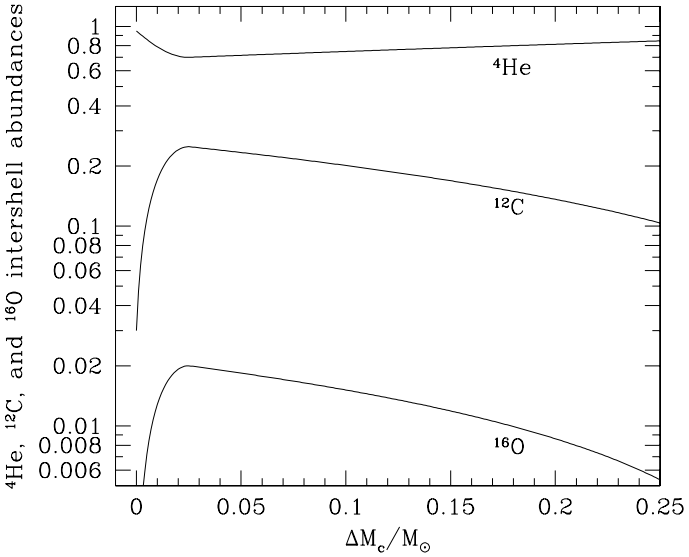

Fig. 9. Chemical composition (^{4}He, ^{12}C, and ^{16}O abundances in mass fraction) of the dredged-up material as a function of the core mass increment during the TP-AGB phase, as predicted by Eqs. (7) and (8).

The coefficients $a_i, i = 1, \ldots, 7$ are given in Table 2 for $Z = 0.019, 0.008$, and 0.004. Interpolation and extrapolation in $\log Z$ are adopted for other metallicities.

2.5.3. Chemical composition of the inter-shell

The abundances of ^{4}He, ^{12}C, and ^{16}O in the intershell region are derived as a function of the core mass growth $\Delta M_c = M_c - M_{c,1TP}$ on the base of nucleosynthesis calculations by Boothroyd & Sackmann (1988). A fit to their Fig. 9 gives:

$$\begin{aligned} X(^4\mathrm{He}) &= 0.95 + 400\,(\Delta M_c)^2 - 20.0\,\Delta M_c \\ X(^{12}\mathrm{C}) &= 0.03{-}352\,(\Delta M_c)^2 + 17.6\,\Delta M_c \\ X(^{16}\mathrm{C}) &= -32\,(\Delta M_c)^2 + 1.6\,\Delta M_c \end{aligned} \quad (7)$$

for $\Delta M_c \le 0.025\,M_\odot$, and

$$\begin{aligned} X(^4\mathrm{He}) &= 0.70 + 0.65\,(\Delta M_c - 0.025) \\ X(^{12}\mathrm{C}) &= 0.25{-}0.65\,(\Delta M_c - 0.025) \\ X(^{16}\mathrm{O}) &= 0.02{-}0.065\,(\Delta M_c - 0.025) \end{aligned} \quad (8)$$

for $\Delta M_c > 0.025\,M_\odot$. These relations are displayed in Fig. 9, where we notice that the fractional mass of primary ^{12}C quickly increases during the first pulses up to a maximum value of 0.25 for $\Delta M_c = 0.025\,M_\odot$. Then it starts to decrease slowly. The same behaviour characterises the evolution of the ^{16}O abundance (with a maximum value of 0.02), while a mirror-like trend is followed by ^{4}He that reaches a minimum value of 0.70.

2.6. Hot-bottom burning nucleosynthesis

HBB takes place in the most massive TP-AGB models, with ($M_i \ge 3.5{-}4.5\,M_\odot$) depending on metallicity, and it corresponds to H-burning, mainly via the CNO cycle, in the depeest layers of their convective envelopes. For the present work we adopt the same treatment of this process as in Marigo et al. (1999) to which we refer the reader for more details.

From an observational point of view, HBB not only makes models more luminous than expected by the core mass-luminosity relation (see Sect. 2.2) but also, more importantly, produces notable chemical changes in the surface chemical composition. One of the most significant and well-known effects played by HBB nucleosynthesis is that of converting C into N, hence delaying or even preventing the formation of C stars.

However, it should be noticed that, under particular circumstances, HBB might instead favour the formation of C stars thanks to the destruction of O in favour of N. This applies to low-metallicity massive models in which the temperature at the base of the envelope is high enough to activate the ON cycle. A few exemplifying cases of models experiencing both the third dredge-up and HBB are discussed in Sect. 3.3 and illustrated in Fig. 21.

It is worth emphasising that, at each time step during the interpulse periods, the elemental abundances in the envelope of TP-AGB models with HBB are determined by solving a network of nuclear reactions (the p-p chains and the CNO tricycle), according to the current temperature and density stratifications given by numerical integrations of a complete envelope model (see Marigo et al. 1998 for a complete description of the method). This allows a consistent coupling of the HBB nucleosynthesis with the structural evolution of the envelope, a technical characteristic that places our synthetic TP-AGB model closer to full TP-AGB models. In fact, as already shown by I04 a parameterised treatment of HBB nucleosynthesis in synthetic TP-AGB calculations turns out to be quite complex and sometimes troublesome for the relatively large number of the parameters involved ($\approx$7), their intrisic degeneracy, and the non-univocity of the calibration.

As an example let us consider one of these quantities that is directly related to the efficiency of HBB, i.e. the temperature at the base of the convective, T_{bce}. I04 (see their Sect. 3.3.4) propose a parametric formalism for T_{bce}, which in turn requires additional parameters to be calibrated on the basis of full TP-AGB calculations.

On the other hand, by means of envelope integrations carried out with our synthetic TP-AGB code, we are able to naturally predict the temporal evolution of T_{bce} during the whole TP-AGB phase, as displayed in Fig. 10 for the ($M_i = 4.0\,M_\odot$, $Z = 0.008$) model. Note the complex behaviour and wide excursion in T_{bce} due to thermal pulses, which are zoomed in the inset. Considering only the quiescent pre-flash stages, that ideally describe the upper envelope of the T_{bce} curve, we see that the temperature steeply rises during the first pulse cycles, then flattens out toward a maximum value, and eventually drastically drops as soon as the envelope mass is significantly reduced by mass loss.

2.7. Pulsation modes and periods

Models for pulsating AGB stars (see, e.g., Fox & Wood 1982) indicate that the dominant growth rate (GR) among different pulsation modes is correlated with luminosity; i.e. modes of higher order have the highest GR at lower luminosities. This means that if we consider, for instance, the fundamental (FM) and first

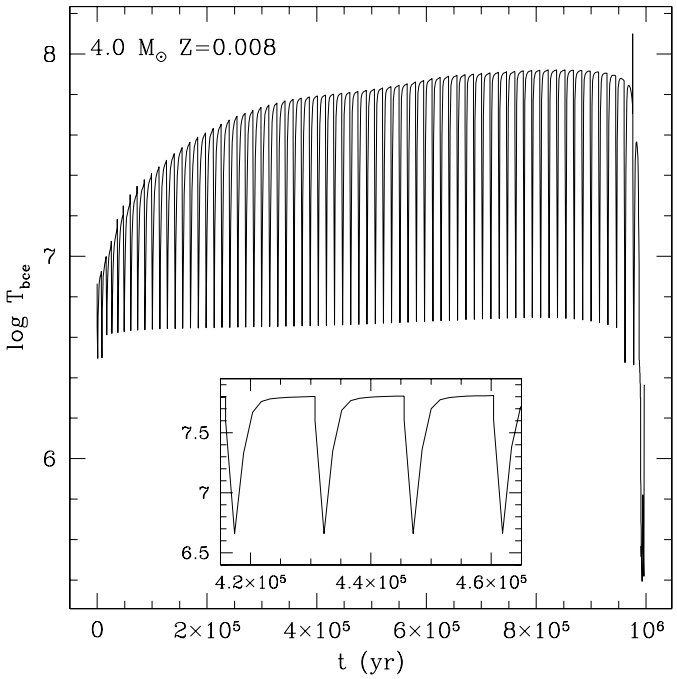

Fig. 10. Evolution of the temperature at the base of the convective envelope during the whole TP-AGB phase of the (4 $M_\odot$, $Z = 0.008$) model that experiences both the third dredge-up and HBB. The inset zooms the temporal behaviour of $T_{\rm bce}$ during few selected pulse cycles.

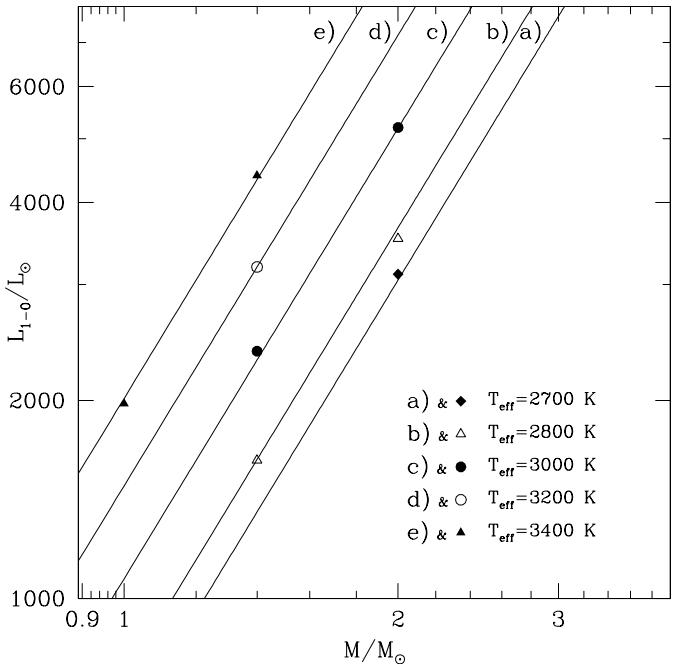

Fig. 11. Critical luminosity L_{1-0} defined by the equality of the growth rates for FO and FM pulsation. Symbols show the predictions of nonadiabatic pulsation models by Ostlie & Cox (1986) for different values of stellar mass and effective temperature. Lines (a–e) are plotted according to the fitting Eq. (10), each of them corresponding to a given $T_{\rm eff}$ at varying stellar mass. See text for more details.

overtone (FOM) modes with growth rates GR_0 and GR_1, respectively, we expect $\mathrm{GR}_1 > \mathrm{GR}_0$ at lower luminosities, while the situation is reversed at higher luminosities.

As a result, making the reasonable assumption that the active pulsation mode among the possible modes is the one corresponding to the highest GR, we derive a picture of pulsation on the AGB: as a star climbs in luminosity it becomes unstable through a sequence of pulsation modes, first exciting those of higher order (i.e. third → second → first overtone) and eventually switching to the fundamental mode (see Lattanzio & Wood 2003).

Due to the lack of sufficient theoretical data on higher order pulsation modes, in this study we limit ourselves to considering the first overtone mode (FOM) and the fundamental mode (FM). We assume that all stellar models start their TP-AGB evolution as FOM pulsators. The transition from the first overtone to the FM pulsation may take place later, provided a minimum luminosity, L_{1-0}, is reached. This critical luminosity is defined by the stage at which the growth rates per unit time, GR, for both modes become equal $(\mathrm{GR}_1 = \mathrm{GR}_0)$[2].

To obtain L_{1-0} we use the results of the linear, nonadiabatic pulsation models for Mira variables calculated by Ostlie & Cox (1986). A good fitting relation (based on their Table 2) providing the critical luminosity as a function of stellar mass and effective temperature is

$$\log L_{1-0}/L_\odot = -14.516 + 2.277 \log M/M_\odot + 5.046 \log T_{\rm eff}. \quad (9)$$

As we notice from Fig. 11 the switch from the FOM to the FM is expected to occur at higher luminosities for higher stellar mass and effective temperature. Since Ostlie & Cox (1986) present models only for solar composition – with $(Y, Z) = (0.28, 0.02)$ – we include a metallicity dependence to Eq. (9) as quantified by Bedijn (1988) on the basis of pulsation models for long-period variables calculated by Fox & Wood (1982) for metallicities $Z = 0.001, 0.01, 0.02$. Following Bedijn (1988, see his Eq. (22)), the transition radius, R_{1-0}, from the FOM to the FM scales as $(Z/0.02)^{-0.042}$; hence we get

$$\log L_{1-0}/L_\odot = -14.516 + 2.277 \log M/M_\odot + 5.046 \log T_{\rm eff} - 0.084 \log(Z/0.02), \quad (10)$$

considering that $L_{1-0} \propto R_{1-0}^2 T_{\rm eff}^4$ for given effective temperature.

The pulsation periods are derived from theoretical (P, M, R)-relations for long-period variables calculated by Fox & Wood (1982). Specifically, FOM periods (P_1) are derived through the analytical fit of the pulsation constant (Wood et al. 1983):

$$\begin{aligned} Q/\mathrm{days} &= (P_1/\mathrm{days})(M/M_\odot)^{1/2}(R/R_\odot)^{-3/2} \quad (11)\\ &= 0.038 \\ &\quad (\text{if } M \geq 3M_\odot;\ \text{or } M = 2M_\odot \text{ and } P_1 < 300 \text{ days};\\ &\quad \text{or } M = 1M_\odot \text{ and } P_1 < 200 \text{ days})\\ &= 0.038 + 2.5 \times 10^{-5}(P_1 - 300)\\ &\quad (\text{if } M = 2M_\odot \text{ and } P_1 > 300 \text{ days})\\ &= 0.038 + 4.5 \times 10^{-5}(P_1 - 150)\\ &\quad (\text{if } M = 1M_\odot \text{ and } P_1 > 150 \text{ days})\\ &= 0.038 + 5.5 \times 10^{-5}(P_1 - 100)\\ &\quad (\text{if } M = 0.7M_\odot \text{ and } P_1 > 100 \text{ days}), \end{aligned}$$

[2] This latter criterion is the same one as proposed by Bedijn (1988) in his synthetic AGB model.

whereas FM periods, P_0, are calculated with

$$\begin{aligned}\log(P_0/\mathrm{days}) &= -2.07 + 1.94\log(R/R_\odot) \\ &\quad -0.9\log(M/M_\odot) \ \ (\mathrm{if}\ M < 1.5M_\odot) \\ &= -2.59 + 2.2\log(R/R_\odot) \\ &\quad -0.83\log(M/M_\odot) - 0.08\log(Z/10^{-3}) \\ &\quad +0.25(Y-0.3) \ \ (\mathrm{if}\ M > 2.5M_\odot)\end{aligned} \tag{12}$$

where Z and Y denote metallicity and helium content (in mass fraction), respectively. These formulae are taken from Groenewegen & de Jong (1994; for $M \le 1.5\ M_\odot$) and Fox & Wood (1982; for $M \ge 2.5\ M_\odot$). For $1.5 < (M/M_\odot) < 2.5$, $\log P_0$ is linearly interpolated using $\log M$ as the independent variable.

2.7.1. A cautionary remark: how to treat pulsation in C-rich models

At present all published pulsation models for long-period variables (e.g., Fox & Wood 1982; Wood 1990; Ya'Ari & Tuchman 1996) are strictly valid only for oxygen-rich chemical compositions, with photospheric C/O < 1, while models suitably constructed for pulsating C stars – and using proper C-rich opacities – are still missing. This means that the extension of the (P, M, R)-relations available in the literature, is not straightforward and possibly wrong. Since one of the main goals of the present study is to provide a more reasonable description of the AGB evolution as a function of the stellar chemical-type, we face the problem of assigning periods to C-rich models. Given the lack of theory, the only remaining approach then comes from the empirical ground.

For instance, assuming that the inertial radius R, which determines the pulsation period, coincides with the photospheric radius – defined by the black-body relation $L = R^2 T_{\rm eff}^4$ (in solar units) – and applying Eqs. (11)–(12) to compute periods of C-rich models, then one would expect that, at a given luminosity, C stars should have larger R owing to their lower $T_{\rm eff}$, hence longer periods than M stars.

As already noted long ago by Wood et al. (1983), this prediction is contradicted by observations since both groups of stars appear to populate the same sequences in the $(M_{\rm bol} - P)$ diagram, as shown for instance in Fig. 6 of Wood et al. (1983; see also Hughes & Wood 1990). This feature has been confirmed by more recent and extended surveys of long-period variables (e.g., Groenewegen 2004; Fraser et al. 2005).

As suggested by Wood et al. (1983), the immediate implication is that, unlike the photospheric radius, the inertial radius of pulsating AGB stars should be largely insensitive to the photospheric C/O ratio. In other words, while the photospheric radius of C stars is expected to be much more extended than that of M stars of the same luminosity due to an opacity effect, the inertial radii of both classes of stars should be quite similar.

For all these reasons, in this work we have simply decided to calculate periods as follows (all quantities are in solar units)

$$R = L^{0.5} T_{\rm eff}^2 \qquad \text{for M-type models with C/O} < 1, \tag{13}$$

which is the inertial radius coincides with the photospheric radius,

$$R = L^{0.5} T_{\rm eff,M}^2 \quad \text{for C-type models with C/O} > 1, \tag{14}$$

which is the inertial radius is calculated by assigning the effective temperature $T_{\rm eff,M}$ that would compete to an M-type model with the same luminosity. In these case $T_{\rm eff,M}$ is derived from envelope integrations, always assuming a fictious oxygen-rich composition (i.e. assuming the solar ratio, C/O = 0.48).

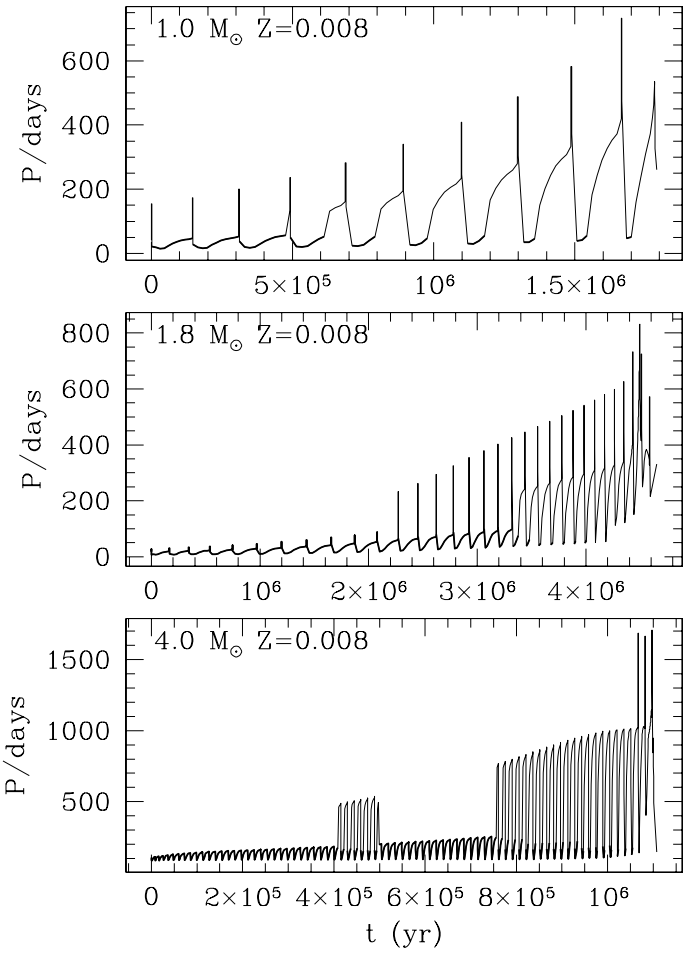

Fig. 12. Evolution of pulsation period along the TP-AGB phase of a few selected models with initial metallicity $Z = 0.008$. First-overtone and fundamental periods, $P = P_1$ and $P = P_0$, are drawn with thick and thin solid lines, respectively.

The predicted period evolution during the whole TP-AGB phase of a few selected models is shown in Figs. 12 and 13. The variations in luminosity and photospheric radius produced by thermal pulses reflect in the quasi-periodic behaviour of P, in substantial agreement with the predictions of detailed AGB models and their pulsation properties (e.g., Vassiliadis & Wood 1993; Wagenhuber & Tuchman 1996). Moreoever, in all models it is very evident the switch from FOM to FM pulsation regime and vice versa, corresponding to a mean change in period by a factor of ∼2. According to the luminosity criterion given by Eq. (10) the mode switching would not correspond to a single event during the TP-AGB evolution, but it could actually take place several times, driven by the luminosity variations produced by thermal pulses. As displayed in Figs. 12 and 13, there might be cases in which the mode transition may occur during the pulse cycle, with the FOM pulsation characterising the low-luminosity dips, and the FM pulsation being recovered at increasing luminosities during the quiescent stages. It should be also noticed that the $T_{\rm eff}$-dependence of L_{1-0} in Eq. (10) favours the switching to the FM pulsation at decreasing effective temperature. This explains the occurrence of a short FM stage experienced by the ($M_{\rm i} = 4.0\ M_\odot$, $Z = 0.008$) model at evolutionary ages $t \approx 5 \times 10^5$ yr, which just corresponds to the transitory fulfillment of the condition C/O > 1 (see Fig. 3), thanks to the effect of the third dredge-up prevailing over that of HBB.

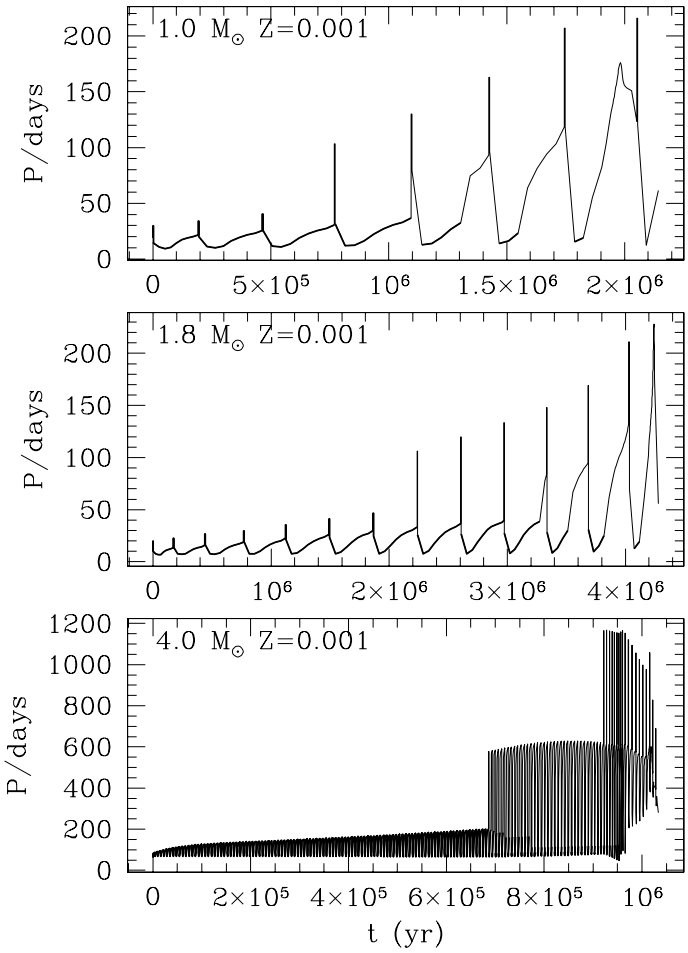

Fig. 13. The same as in Fig. 12, but for metallicity $Z = 0.001$.

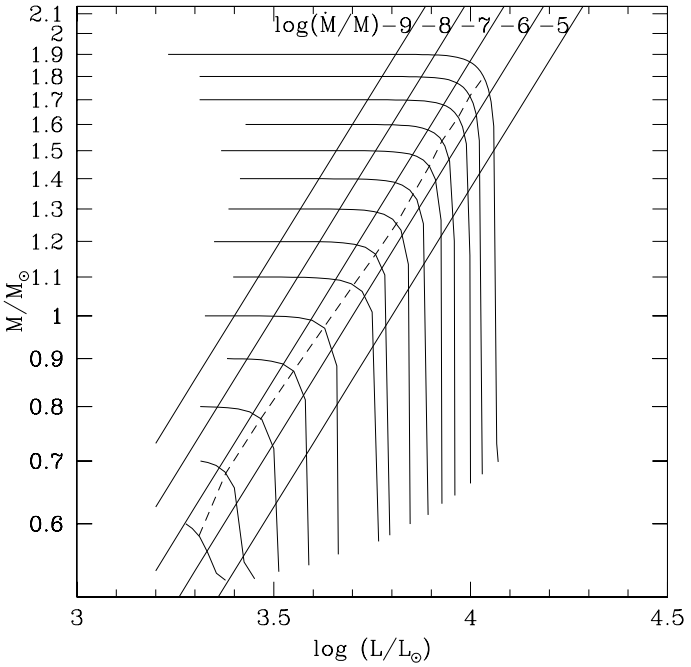

Fig. 14. Mass evolution of O-rich TP-AGB models with $Z = 0.019$ as a function of luminosity, with mass-loss rates calculated on the base of Bowen & Willson (1991) dynamical atmospheres for Miras including dust. The five parallel solid lines define the approximate loci of constant $\dot{M}/M$ (in units of yr^{-1}), corresponding to evolutionary slopes $\mathrm{d}\log M/\mathrm{d}\log L = -0.0018, -0.018, -0.18, -1.8, -18$ (from left to right). The dashed line is the "cliff" line, along which $\mathrm{d}\log M/\mathrm{d}\log L = 1$ and $\dot{M}/M = 5.67 \times 10^{-7}\ \mathrm{yr}^{-1}$.

2.8. Mass-loss rates

Mass-loss rates, $\dot{M}$, during the TP-AGB evolution are calculated in a different fashion depending on whether a stellar model is oxygen-rich or carbon-rich.

2.8.1. O-rich models

In the C/O < 1 case we use the results of dynamical atmospheres including dust for long-period variables calculated by Bowen & Willson (1991). The grid of model atmospheres is suitably constructed for oxygen-rich Mira-type stars with solar metallicity, and it covers the ranges of initial masses $M_\mathrm{i} = 0.7{-}2.4\,M_\odot$ and periods $P = 150{-}800$ days. Pulsation is assumed to occur in the FM.

By suitably combining their dynamical calculations and with a few basic formulas[3] to describe the evolution of stellar parameters on the AGB, Bowen & Willson (1991) derived a relationship between the mass-loss rate $\dot{M}$ and the slope of a stellar AGB evolutionary track in the $\log M$–$\log L$ diagram:

$$\frac{\dot{M}}{M} = 5.65 \times 10^{-7}\,\frac{\mathrm{d}\log M}{\mathrm{d}\log L} \qquad \left[\mathrm{yr}^{-1}\right] \tag{15}$$

where M and L are in solar units, and $\dot{M}$ is given in $M_\odot\ \mathrm{yr}^{-1}$.

To summarise, the adopted procedure to specify $\dot{M}$ for an oxygen-rich AGB model is as follows. Given the current values of stellar mass M, photospheric radius R, and pulsation period P (obtained according to Sect. 2.7), we derive the corresponding luminosity used by Bowen & Willson (1991, their Eq. (3)) in their computation of model atmospheres. Then, for any specified combination of (L, M), the evolutionary slope $\mathrm{d}\log M/\mathrm{d}\log L$ is obtained by interpolation between grid points defined by the lines of constant $\dot{M}/M$ shown in Fig. 2 of Bowen & Willson (1991). Finally the mass-loss rate follows from Eq. (15).

Figure 14 shows a grid of TP-AGB evolutionary tracks with C/O < 1 in the $\log M$–$\log L$ diagram. We plot only models at the quiescent stages of pre-flash luminosity maximum. Along each track, the stellar mass stays constant until an abrupt change of slope takes place. This marks the onset of the superwind mass loss, which determines the quick ejection of the whole envelope and the termination of the AGB phase. The sequence of these sharp corners at varying M and L form the so-called "cliff" line, as designated by Willson (2000). It is defined by the condition $\mathrm{d}\log M/\mathrm{d}t \sim \mathrm{d}\log L/\mathrm{d}t$ and it corresponds to a critical mass loss rate $\dot{M}_\mathrm{crit} \sim 5.67 \times 10^{-7} \times M$ in units of $M_\odot\ \mathrm{yr}^{-1}$. Once it reaches the cliff point, the star enters the superwind phase.

As anticipated by Bowen & Willson (1991) and thoroughly discussed by Willson (2000), at decreasing metallicity the mass-loss rate of an oxygen-rich AGB star is affected by two factors, namely: i) less efficient dust production due to the lower abundances of involved elemental species, and ii) more compact structure, i.e. smaller photospheric radius at given luminosity. It turns out that the latter effect is the largest, producing a shift of the cliff line to higher L for lower Z (see Fig. 9 in Willson 2000). Following Bowen & Willson (1991) for $Z < 0.1Z_\odot$, the onset of

[3] These refer to the period-mass-radius relation for FM pulsation, the radius-luminosity-mass relation, and the core mass-luminosity relation.

the superwind takes place at a critical luminosity, approximately given by

$$L_{\rm SW}(Z) = L_{\rm SW}(Z_\odot) + \Delta L_{\rm SW}, \quad (16)$$

where

$$\Delta L_{\rm SW} = 0.12{-}0.13\ \log(Z/Z_\odot). \quad (17)$$

A few comments should be made at this point. First, we should keep in mind that the results obtained by Bowen & Willson (1991) and illutrated in the key ($\log M$ vs. $\log L$) diagram (their Fig. 2) are not only dependent on the details of their model for dynamical atmospheres, but they also rely on the adopted relations to describe the underlying AGB evolution for various choices of the stellar mass. This fact introduces some inconsistency in our calculations as we are dealing with different synthetic TP-AGB models (e.g., different core mass-luminosity relation). Nevertheless the adopted approach is the best possible one for the available theoretical information. Moreover, it produces results that considerably improve the comparison between predictions and observations (see Sect. 3.5).

Second, we recall that the Bowen & Willson (1991) calculations are strictly valid for FM pulsation. There is no extended analysis of the same kind devoted to pulsation in modes of higher order. A limited set of dynamical models for FOM pulsation including dust are presented by Bowen (1988). By comparing the mass-loss rates calculated by Bowen (1988) for FM (Table 6) and FOM models (Table 8) with the same given combination of stellar mass, radius and effective temperature[4], we obtain the behaviour shown in Fig. 17.

We notice that the trend is not monothonic, as $\dot{M}$ for $P = P_1$ (hereafter $\dot{M}_1$) may be lower or higher than $\dot{M}$ for $P = P_0$ (hereafter $\dot{M}_0$) depending on stellar mass. Moreover, the peak in the $\dot{M}_1/\dot{M}_0$ ratio appears to become higher and to shift towards lower masses at decreasing P_0. Polynomial fits of $\dot{M}_1/\dot{M}_0$ for three values of P_0 are derived assuming the rational form

$$\frac{\dot{M}_1}{\dot{M}_0} = \frac{b_1 + b_2 M + b_3 M^2}{c_1 + c_2 M + c_3 M^2}. \quad (18)$$

The coefficients a_i and b_i are given in Table 3.

In practice, in order to estimate the mass-loss rate of a TP-AGB star pulsating in the FOM mode we proceed as follows. For given stellar mass, radius, and luminosity, we compute the period P_0 via Eq. (12) and the corresponding mass-loss rate $\dot{M}_0$ according to Sect. 2.8. Then we apply Eq. (18) to derive $\dot{M}_1$ (linear interpolation or extrapolation in $\log P$ are adopted between grid points at given M).

Being aware that this recipe based on the few FOM models calculated by Bowen (1989) does not allow a complete picture of mass loss to be derived under FOM pulsation, nevertheless it represents a first attempt to address the question. Moreover, this is more likely to be a realistic approach than simply scaling the mass-loss rate for FM pulsators for $P = P_1 \approx P_0/2.2$ (cf. Fig. 23), which would always lead to very low mass-loss rates. On the contrary, observations indicate that low-period AGB variables, like the semiregulars, are characterised by mass-loss rates comparable with those of Miras, up to few $10^{-7}\,M_\odot\ {\rm yr}^{-1}$ (e.g., Olofsson et al. 2002). If these stars are assigned a pulsation mode different from the FM, likely the FOM, as currently suggested (see Lattanzio & Wood 2003), then this would imply that i) either the $\dot{M}(P)$ relation depends on the pulsation mode, or ii) $\dot{M}$ is independent of P and the observed correlation between $\dot{M}$ and P just hides the true dependence on other basic stellar parameters, like mass, luminosity, and effective temperature. It is clear that detailed analyses of dynamical FOM pulsating atmospheres should be of paramount importance in investigating this point.

Table 3. Coefficients for Eq. (18).

	P_0/days		
	350	500	700
b_1	–0.2946	–0.2581	0.4167
b_2	0.5488	0.1089	2.1701
b_3	2.1750E-02	0.5608	–0.4167
c_1	1.3309	3.9290	0.8738
c_2	–3.0054	–7.2055	–6.0280
c_3	1.7392	3.4831	25.6437

2.8.2. Carbon-rich models

In the C/O $>$ 1 case we exploit the results of pulsating dust-driven wind models for carbon-rich chemistry, as developed by the Berlin group (Fleisher et al. 1992; Sedlmayr & Winters 1997; Winters et al. 2000; Wachter et al. 2002; Winters et al. 2003, and references therein). Extended grids of models are suitably constructed for carbon-rich AGB stars, yielding the mass-loss rate as a function of main stellar parameters, such as effective temperature (2200–3000 K), luminosity (3000–24 000 $L_\odot$), mass (0.8–1.8 $M_\odot$), photospheric C/O ratio (1.20–1.80), and pulsation period (100–1000 days). According to the detailed investigation by Winters et al. (2000, 2003), one can schematically distinguish two dynamical regimes for the stellar outflows.

The first regime refers to the so-called B-type models, and it should apply to low-luminosity, short-period, high-effective temperature red giants, for which the dominant mass-loss driving mechanism is stellar pulsation, while radiation pressure on dust grains plays a reduced role. In fact for this class of models, radiation pressure alone is not able to produce an outflow, with such a condition expressed by $\alpha < 1$[5]. During this regime tenuous winds are generated, characterised by low terminal velocities ($v_\infty < 5$ km s^{-1}) and low mass-loss rates, never exceeding a critical value of $\dot{M}_{\rm crit} \approx 3 \times 10^{-7}\,M_\odot\ {\rm yr}^{-1}$.

The subsequent development of a stable dust-driven wind from a carbon star (with $\dot{M} > \dot{M}_{\rm crit}$) requires a minimum luminosity $L_{\rm SW}$, such that the outward acceleration provided by radiation pressure on dust exceeds the inward gravitational pull ($\alpha \geq 1$). According to Winters et al. (2000) models, this critical luminosity depends mainly on stellar mass and effective temperature. As soon as $L \geq L_{\rm SW}$, a carbon star is expected to enter the dust-driven-wind regime, described by the so-called A-type models, with mass-loss rates in the typical range $3 \times 10^{-7} \lesssim \dot{M} \lesssim 10^{-4}\,M_\odot\,{\rm yr}^{-1}$, and terminal velocities in the range $5 \lesssim v_\infty \lesssim 40$ km s^{-1}.

The picture just depicted leads us to adopt the following recipe to calculate the mass-loss rate for carbon-rich models evolving on the TP-AGB. First we need to specify the critical luminosity $L_{\rm SW}$ that separates the two wind regimes. Based on

[4] For assigned fundamental-mode periods $P_0 = 350, 500, 700$ days, and stellar masses, $M = 0.8, 1.0, 1.2, 1.6, 2.0\,M_\odot$, the corresponding radii and first-overtone mode periods are derived from the period-mass-radius relationships by Ostlie & Cox (1986), while $T_{\rm eff} = 3000$ K is assumed in all cases.

[5] The standard notation of dynamical wind models defines $\alpha \equiv a^{\rm rad}/a^{\rm grav}$, the ratio of the radiative acceleration over the gravitational one.

wind models calculated by Schröder et al. (1999) – with transition properties between the B and A classes – Schröder et al. (2003) propose an approximate relation, giving $L_{\rm SW}$ as a function of stellar mass M and effective temperature $T_{\rm eff}$:

$$\log(L_{\rm SW}/L_\odot) = 3.8 + 4(\log T_{\rm eff} - 3.45) + \log(M/M_\odot). \quad (19)$$

This relation is derived from a small subset of wind models for various choices of stellar mass and effective temperature, while adopting the same period, $P = 400$ days, and carbon-to oxygen ratio, C/O = 1.3.

In the present work an attempt has been made to refine this relation by also including a dependence on the pulsation period P. To this aim we use a sample of pulsating wind models computed by Winters et al. (2000; their Tables 6–9) at varying input parameters, namely, stellar mass M, effective temperature $T_{\rm eff}$, pulsation periods P (in days), carbon-to-oxygen ratio C/O, and piston velocity[6] $\Delta v_{\rm p}$.

From these data we derive the stellar luminosity at which the time-averaged (over a few pulsation periods) $\alpha \approx 1$, as a function of M, $T_{\rm eff}$, and P (in days), while we consider fixed both the carbon-to-oxygen ratio (C/O = 1.2), and the piston velocity ($\Delta v_{\rm p} = 5$ km s^{-1}). The resulting fitting relation reads

$$\begin{aligned}\log(L_{\rm SW}/L_\odot) \;=\; & 3.796 + 6.614\log(T_{\rm eff}/2800) \\ & +1.096\log(M/M_\odot) - 1.728\log(P/400).\end{aligned} \quad (20)$$

For the sake of comparison, Fig. 18 displays $L_{\rm SW}$ as a function of stellar mass, as predicted for $T_{\rm eff} = 2800$ K by our proposed fit (Eq. (20)) for three choices of the pulsation period, and by Eq. (19) without period-dependence suggested by Schröder et al. (2003). We note that our proposed formula recovers the Schröder et al. (2003) relation well for $P = 400$ days, while predicting a significant sensitiveness of $L_{\rm SW}$ to period changes, i.e. the onset of the dust-superwind should occur at lower luminosities for longer periods.

As long as $L < L_{\rm SW}$, the mass-loss rate is calculated as a function of the near infrared $J - K$ colour

$$\log[\dot{M}/(M_\odot\,{\rm yr}^{-1})] = \frac{-6.0}{J-K+0.1} - 4.0, \quad (21)$$

according to the semi-empirical calibration by Schröder et al. (2003). The above equation is the best match to the mass-loss rates of Galactic disk C stars belonging to the Le Bertre (1997) sample with moderate mass loss (with colours in the range $2.5 \lesssim J - K \lesssim 4$), which is before the full development of the dust-driven superwind.

The $J - K$ colour for these models is in turn computed with the aid of the relation

$$(J-K) = 17.32 - 4.56\log T_{\rm eff} + 0.052\,{\rm C/O} \quad (22)$$

proposed by Marigo et al. (2003). The above equation extends the original colour-$T_{\rm eff}$ transformation for C stars by Bergeat et al. (2001), by introducing a C/O-dependence to account for the effect molecular blanketing on the spectra of these stars.

Then, once the luminosity of a carbon-rich model overcomes $L_{\rm SW}$, the dust-driven superwind is assumed to start. This phase is described on the base of pulsating wind models presented by Wachter et al. (2002), in which the driving mechanism of mass loss is the radiation pressure on dust grains. From those models we derive a fitting relation, expressing the mass-loss rate as a function of stellar luminosity L, effective temperature $T_{\rm eff}$, mass M, pulsation period P, and photospheric C/O ratio (the piston amplitude is assumed $\Delta v_{\rm p} = 5$ km s^{-1} for all models)

$$\begin{aligned}\log[\dot{M}/(M_\odot\,{\rm yr}^{-1})] \;=\; & -4.529 \\ & -6.849\,\log(T_{\rm eff}/2600\,{\rm K}) + 1.527\,\log(L/10^4\,L_\odot) \\ & -1.997\,\log(M/M_\odot) - 0.995\,\log(P/650\,{\rm days}) \\ & +0.672\log\left(\frac{\rm C/O}{1.5}\right).\end{aligned} \quad (23)$$

The numerical coefficients are quite similar to those of the fitting formula for $\dot{M}$ already proposed by Wachter et al. (2002; see their Eq. (1)) obtained from the same set of wind models. We note that Eq. (23) contains an explicit dependence of $\dot{M}$ on the C/O ratio that is neglected in the Wachter et al. formula. Our choice is motivated by the fact that, although the influence of C/O is expected to be rather weak for relatively low ratios (<2 as is the case of Galactic C stars), it may instead become important for larger C/O ratios, e.g., in carbon stars belonging to metal-poor populations.

A few examples of the predicted mass-loss rates are displayed in Figs. 15 and 16. In all cases, regardless of the C/O value, we note that i) the mass-loss rate is modulated by the variations in luminosity and effective temperature driven by the He-shell flashes, ii) most of the stellar mass is lost during the quiescent stages of high luminosity preceeding the occurrence of the thermal pulses, and iii) the super-wind regime is attained during the FM pulsation ($P = P_0$).

3. Basic model predictions

The synthetic model just described in Sect. 2 has been applied to calculate the TP-AGB evolution of an extended set of stellar models, with initial masses in the interval 0.5–5.0 $M_\odot$, and for 7 choices of metallicity, Z = 0.0001, 0.0004, 0.001, 0.004, 0.008, 0.019, 0.03. The TP-AGB phase is followed from the first thermal pulse up to the complete ejection of the envelope by stellar winds.

In the following we describe the basic properties of our TP-AGB models, emphasising the new aspects that derive from a number of updates applied to our synthetic code (described in Sect. 2), the most important of which are: (i) an improved description of the pulsation periods, so as to account for the switching from the FOM to the FM of pulsation; (ii) a better recipe for predicting the mass-loss rates, distinguishing between O-rich and C-rich models; (iii) the use of variable molecular opacities; (iv) a more detailed treatment of the third dredge-up and HBB.

3.1. Transition luminosities

The classical picture of TP-AGB evolution is one of luminosity generally increasing with time as the core mass grows along the evolution. This picture has already been demonstrated to fail under a series of circumstances (e.g., flash-driven luminosity variations, very deep dredge-up, extinction of HBB, etc.); however, it is still useful to define a few transition luminosities that mark the onset of particular regimes during the TP-AGB phase. The several panels in Fig. 19 show a few characteristic luminosities

[6] In the piston-approximation, commonly used in pulsating wind models, the piston amplitude $\Delta v_{\rm p}$ denotes the velocity amplitude of the innermost grid point, assumed to vary sinusoidally over the pulsation period P.

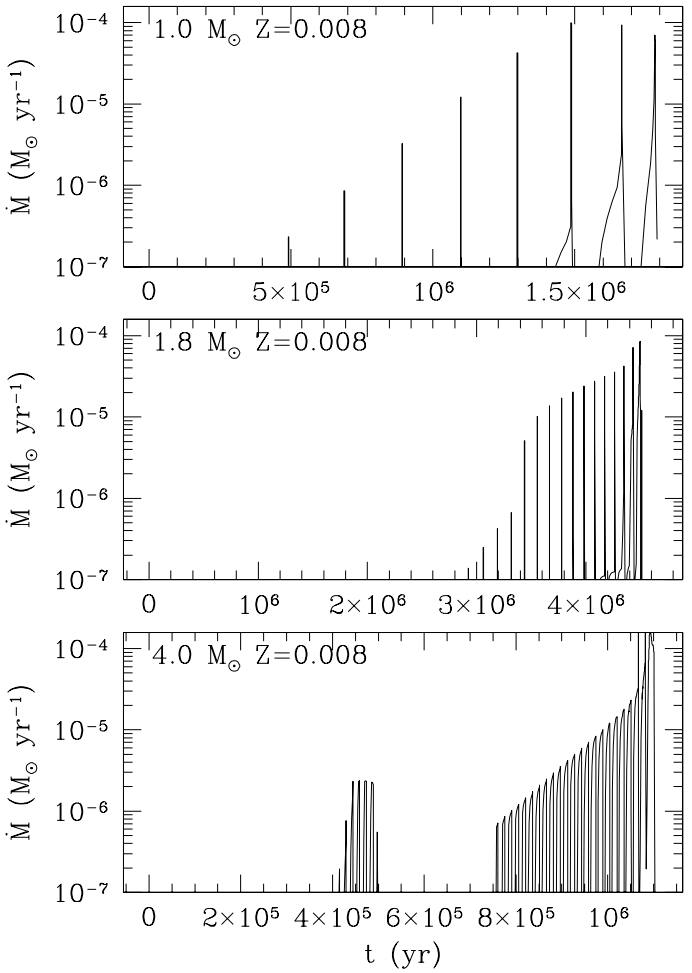

Fig. 15. Evolution of the mass-loss rate during the TP-AGB phase of a few selected models.

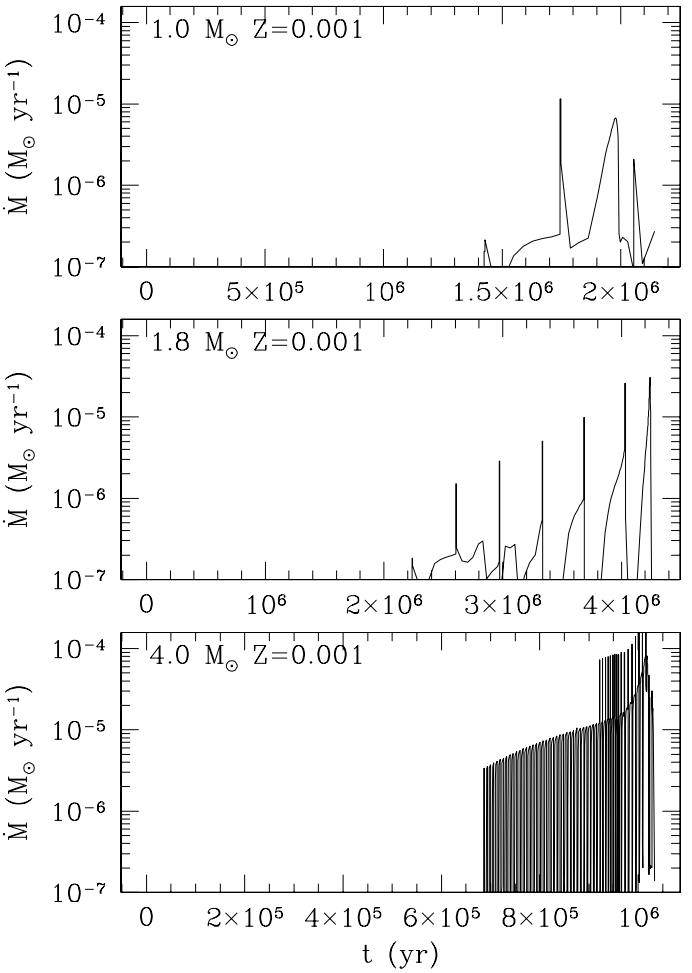

Fig. 16. The same as in Fig. 15, but for metallicity $Z = 0.001$.

as a function of the stellar mass, for the 7 metallicities explored in this work. These critical luminosities correspond to the quiescent pre-flash values at the stages of:

- the first termal pulse, L_{1TP};
- the switch from fundamental mode to first-overtone mode pulsation, $L_{P_1} - L_{P_0}$;
- the transition from oxygen-rich to carbon-rich surface chemical composition, $L_{\rm M-C}$;
- the onset of the superwind phase of mass loss, $L_{\rm SW}$, with $\dot{M} > 5 \times 10^{-7}\, M_\odot\, {\rm yr}^{-1}$;
- the luminosity at the end of the AGB phase, $L_{\rm AGB-tip}$.

From comparing the various panels in Fig. 19 we derive the following indications:

- The "chemical" transition from M- to C-type takes place at lower luminosities with decreasing Z. Moreover, the minimum mass to become a carbon star decreases with metallicity, being $\sim$2.0 $M_\odot$ for $Z = 0.019$ and $\sim$0.8 $M_\odot$ for $Z \le 0.001$.
- The transition from the FOM to the FM pulsation occurs at higher luminosities with decreasing Z. In particular, low-mass stars (say with $M_{\rm i} \lesssim 1{-}1.5\, M_\odot$) of low Z enter the TP-AGB phase as FOM pulsators, while they should already appear as FM pulsators at solar or super-solar metallicity. At higher masses the transition to FM pulsation always takes place during the TP-AGB phase, regardless of Z.
- Combining the above trends for $L_{P_1-P_0}(M_{\rm i}, Z)$ and $L_{\rm M-C}(M_{\rm i}, Z)$, it follows that at lower metallicities carbon

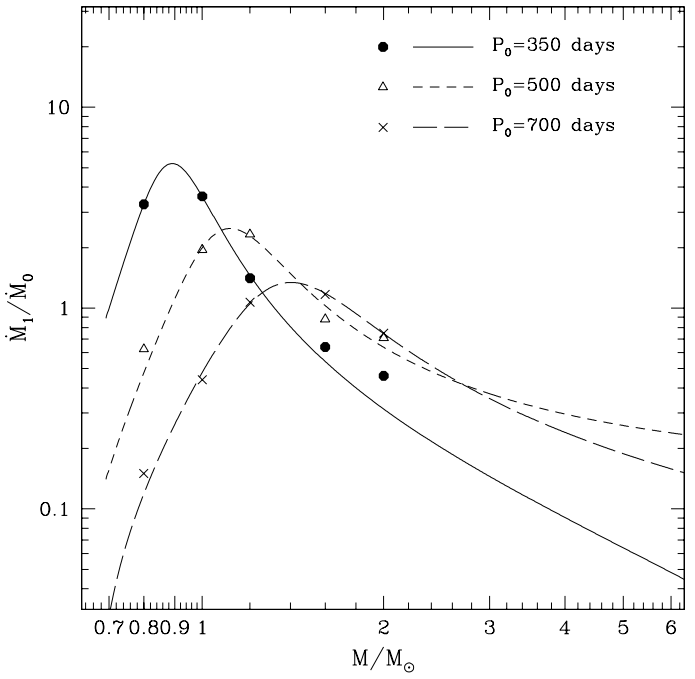

Fig. 17. Predicted ratio between the mass loss rates $\dot{M}_1$ and $\dot{M}_0$, under the assumption of FOM and FM pulsation, respectively, as a function of the stellar mass according to the dynamical atmosphere models calculated by Bowen (1988). Three groups of models, characterised by the same P_0, are shown together with the corresponding polynomial fits.

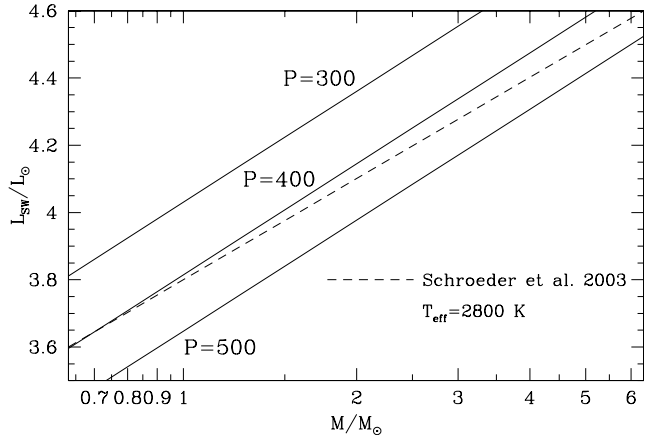

Fig. 18. Critical luminosity for the onset of the super-wind in C-rich models as a function of the initial stellar mass, according to Eq. (19) (dashed line) for $P = 400$ days, and Eq. (20) (solid line) for three choices of P, as indicated. In all cases the effective temperature is set equal to 2800 K.

stars of any mass should first populate the FOM sequence and then jump to the FM sequence in the $P - L$ diagram. At increasing metallicities, the $L_{\rm M-C}$ transition tends to occur at higher luminosities at any given stellar mass, so that carbon stars should predominantly appear as FM pulsators.

– The $L_{\rm SW}$ for both oxygen-rich and carbon-rich models is always attained after the transition from FOM to FM pulsation, and it practically determines the final luminosity, $L_{\rm tip-AGB}$ attained at the termination of the AGB phase.

– For carbon-rich models, $L_{\rm SW}$ is very close to the $L_{\rm M-C}$ transition at higher metallicities; e.g., as a star with initial $Z \geq 0.019$ becomes a carbon star the significant decrease in $T_{\rm eff}$ favours the quick development of the dusty superwind regime. At decreasing metallicities, the surface cooling effect caused by the transition from M- to C-type domain is less pronounced, so that the onset of the superwind is delayed.

– For oxygen-rich models $L_{\rm SW}$ takes place, on average, at higher luminosities with decreasing Z due to the higher $T_{\rm eff}$. We note that at very low metallicities, say $Z \leq 0.001$, low-mass models with $M_{\rm i} \leq 0.8\,M_{\odot}$ do not reach the minimum mass-loss rates ($\approx 5 \times 10^{-7}\,M_{\odot}$ yr^{-1}) required for the development of the dusty superwind. In these cases the reduction of the envelope mass and the consequent termination of the AGB phase are mostly determined by the core mass growth, i.e. the rate of outward displacement of the H-burning shell.

3.2. TP-AGB tracks in the H-R diagram

Figure 20 displays the complex morphology of the TP-AGB tracks in the H-R diagram at varying initial stellar mass and metallicity. Again, for the sake of simplicity, only quiescent stages – i.e. pre-flash luminosity maxima – are considered.

As long as the mass loss remains so modest that the TP-AGB evolution can be safely considered at constant mass, the main parameter that affects the evolution in effective temperature is the surface chemical composition, specifically the C/O ratio (see Sect. 3.3). Lower-mass stars that do not experience the third dredge-up, hence always remain O-rich, are characterised by a slight decrease in $T_{\rm eff}$ as they evolve at increasing luminosities along their tracks, with a slope $\mathrm{d}\log L/\mathrm{d}\log T_{\rm eff}$ essentially determined by the stellar mass and initial metallicity.

This behaviour changes drastically as a model makes the transition from the O-rich to the C-rich configuration, which is is accompanied by a marked displacement toward lower effective temperatures (thick lines). As already discussed, this is the direct result of the enhanced molecular opacities as soon as as the photospheric ratio passes from C/O < 1 to C/O > 1. We also note that at decreasing metallicity, on average, the C-rich tracks describe a wider excursion in $T_{\rm eff}$, compared to C-rich models with higher Z. This is due to the fact that at lower Z the transition to the C-star domain takes place earlier, so that models leave the O-rich branch toward lower $T_{\rm eff}$s already during the initial stages of the TP-AGB.

One remark should be made at this point. There are some intermediate mass models that, after having become carbon-rich as a consequence of the third dredge-up, are re-converted to the oxygen-rich configuration due to the prevailing effect of HBB (see Sect. 3.3). This is the case, for instance, of the ($4\,M_{\odot}, Z = 0.008$) and ($3.5\,M_{\odot}, Z = 0.004$) models. As shown in Fig. 20 the consequence of such sequence of chemical transitions (C/O < 1 → C/O > 1 → C/O < 1) produces visible loops in the H-R diagram.

At increasing mass and metallicity, say $M_{\rm i} > 4\,M_{\odot}$ and $Z > 0.004$, TP-AGB tracks do not describe a significant cooling in $T_{\rm eff}$ as HBB prevents the C/O ratio to increase above unity (except in the very last stages). However, we should point out that at very low metallicities ($Z \leq 0.001$) the role of HBB in keeping the surface C/O below 1 may not be effective any longer. Rather, efficient nuclear burning at the base of the convective envelope may itself favour the formation of C-rich models via the activation of the ON cycle, as oxygen begins to be efficiently burnt in favour of nitrogen (see Fig. 21). Due to this, metal-poor tracks of higher masses describe in Fig. 20 pronounced excursions toward lower $T_{\rm eff}$.

Finally, it is worth noticing that the luminosity evolution of more massive models is significantly affected by the occurrence of HBB. This process makes these models over-luminous compared to what is predicted by the core mass-luminosity relation in quiescent conditions. As we see in Fig. 20, even though their core mass does not essentially grow because of the deep dregde-up, the corresponding tracks are characterised first by a relatively steep rise in luminosity as a consequence of HBB. Then, after reaching a maximum the tracks exhibit a final decline in luminosity, finally converging to the values predicted by the core mass-luminosity relation. This takes place at the onset of the superwind regime of mass loss, when the drastically reduced envelope mass determines the extinction of HBB.

3.3. Surface chemical composition

As already mentioned in Sect. 3.2, one key parameter that controls the morphology of the TP-AGB tracks in the H-R diagram is the photospheric C/O ratio, mainly affecting the evolution in $T_{\rm eff}$. This latter may remain unaltered during the whole TP-AGB phase – as is the case of lower mass models –, or it may be affected by the third dredge-up and HBB – as in the most massive models (refer to Sect. 2.6).

It is interesting to compare a few emblematic cases, illustrating the evolution of the CNO abundances and the C/O ratio in the convective envelope of models with different masses and metallicities. The results are schematically summarised as follows.

Models that experience only the third dredge-up show a progressive increase in the ^{12}C abundance, hence the C/O ratio that may overcome unity, thus leading to the formation of carbon

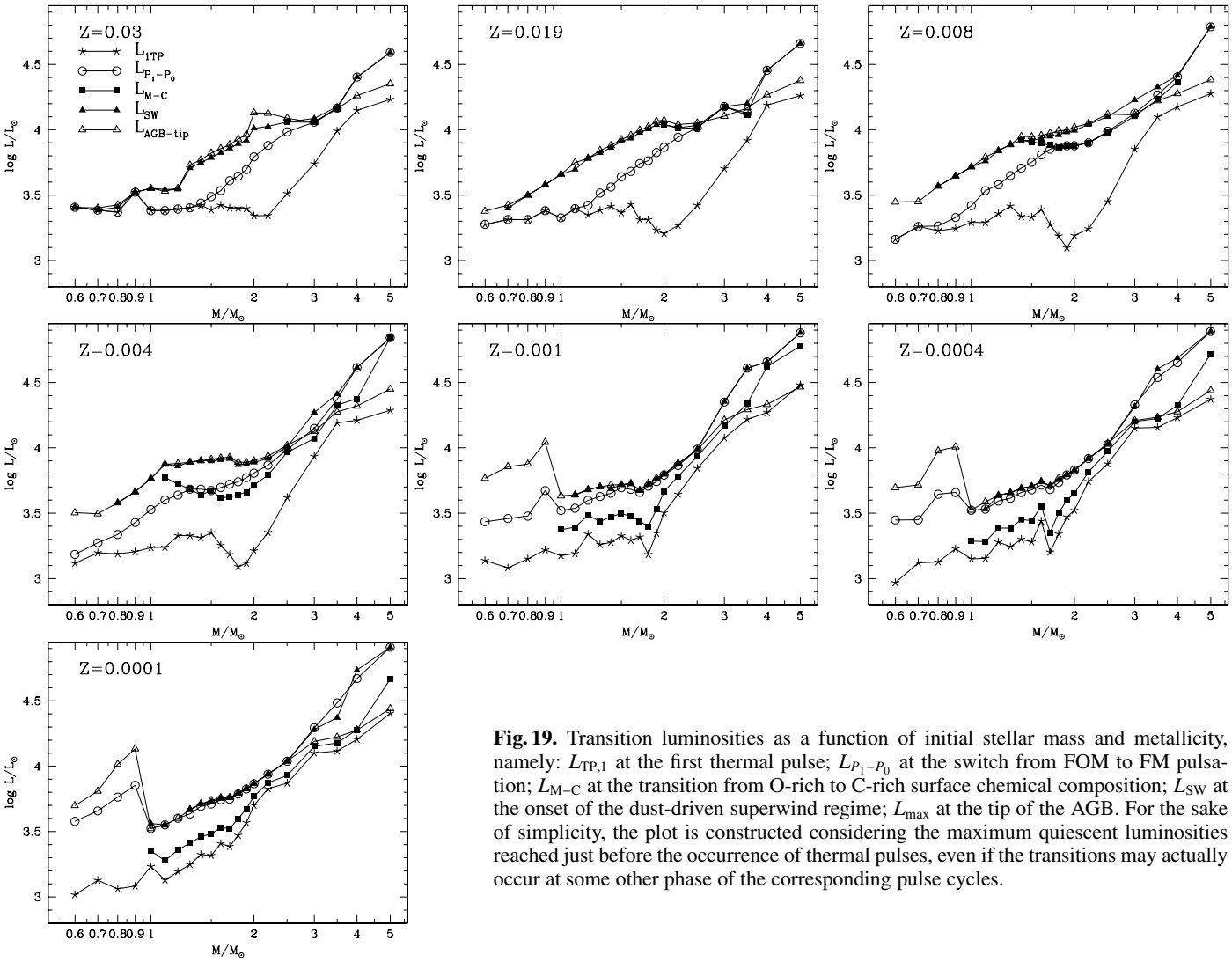

Fig. 19. Transition luminosities as a function of initial stellar mass and metallicity, namely: $L_{\rm TP,1}$ at the first thermal pulse; $L_{P_1-P_0}$ at the switch from FOM to FM pulsation; $L_{\rm M-C}$ at the transition from O-rich to C-rich surface chemical composition; $L_{\rm SW}$ at the onset of the dust-driven superwind regime; $L_{\rm max}$ at the tip of the AGB. For the sake of simplicity, the plot is constructed considering the maximum quiescent luminosities reached just before the occurrence of thermal pulses, even if the transitions may actually occur at some other phase of the corresponding pulse cycles.

stars. This case applies, for instance, to the $M_{\rm i} = 2.5\,M_\odot$ models shown in the bottom panels of Fig. 21. Note that the duration of the C-star phase is much longer for $Z = 0.008$ than for $Z = 0.019$. No important variations are expected in the abundances of N and O.

In models that experience both the third dredge-up and HBB the evolution of the surface CNO abundances depends on the competition between the two processes. We distinguish three possible channels.

1) If the third dredge-up initially dominates, then the C/O ratio is allowed to increase and the model enters the C-star domain. The situation may be later reversed as HBB becomes more and more efficient in converting C in favour of N, so that the C/O ratio falls below unity. This case applies to the models with intermediate mass, like the $M_{\rm i} = 3.5\,M_\odot$, $Z = 0.004$ one shown in the middle-left panel of Fig. 21.

It is worth mentioning here that the evolution of these models, hence their nucleosynthesis, strongly depends on the adopted molecular opacities *and* mass-loss rates. In fact, as shown by Marigo (2007), the use of a mass-loss formalism highly sensitive to $T_{\rm eff}$, e.g. Vassiliadis & Wood (1993), coupled to *variable* molecular opacities could weaken, or even quench, HBB shortly after the surface C/O ratio has overcome unity as a consequence of the third dredge-up. In that case, C/O does not decrease any longer and the model is expected to remain C-rich until the end of its evolution (see Fig. 2 in Marigo 2007). This specific point deserves a more detailed investigation.

2) The early transition to the C-star phase may even be prevented in models of higher mass when HBB is already strong enough to burn the newly dredged-up ^{12}C. These models are then predicted to keep the surface C/O ratio below unity for the whole TP-AGB phase, possibly except for the very last stages of intense mass loss when HBB stops and the third dredge-up makes them appear as obscured carbon stars (van Loon et al. 1997; Frost et al. 1998). This picture is exemplified, for instance, by the $M_{\rm i} = 4.5\,M_\odot$, $Z = 0.004$ and $M_{\rm i} = 5.0\,M_\odot$, $Z = 0.008$ models displayed respectively in the middle-right and bottom-left panels in Fig. 21.

3) At very low metallicities, HBB may even concur – together with the third dredge-up – to favour the formation of massive carbon stars. In fact, the high temperatures ($\gtrsim 7.9 \times 10^7$ K) reached at the base of the convective envelope lead to the activation of the ON-cycle, with the consequent conversion of oxygen into nitrogen. In this case the rise of the surface C/O ratio is mainly due to the depletion of the initial abundance of oxygen. According to our calculations, this condition is met by models with $M_{\rm i} \gtrsim 4.0\,M_\odot$ and $Z \lesssim 0.001$ (see Ventura et al. 2002, for similar results). An example is given by the $M_{\rm i} = 5.0\,M_\odot$, $Z = 0.0004$, shown in the bottom-right panel of Fig. 21. We see that, after an initial decrease in carbon, the CN

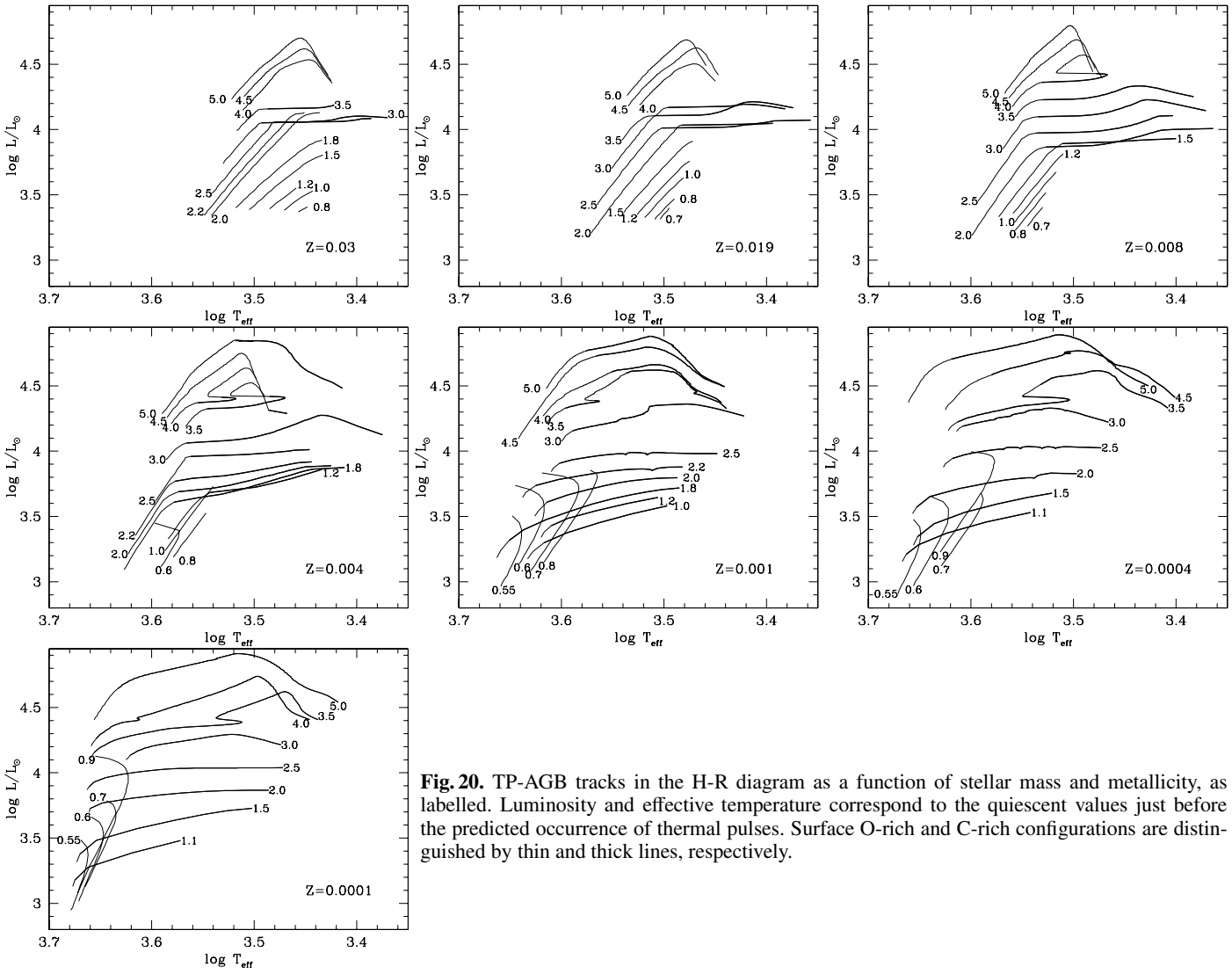

Fig. 20. TP-AGB tracks in the H-R diagram as a function of stellar mass and metallicity, as labelled. Luminosity and effective temperature correspond to the quiescent values just before the predicted occurrence of thermal pulses. Surface O-rich and C-rich configurations are distinguished by thin and thick lines, respectively.

cycle attains its equilibrium regime – i.e. both $^{12}C/^{13}C$ and C/N reach their equilibrium values – and on average carbon starts to increase steadily. Then, the activation of the ON cycle leads to a significant drop in oxygen, which makes the C/O ratio increase above unity. Subsequently the ON-cycle goes to equilibrium as well so that carbon remains more abundant than oxygen despite the steady increase in oxygen.

3.4. Duration of the TP-AGB phase

Figure 22 shows the predicted TP-AGB lifetimes for both the oxygen-rich (with $M_{\rm bol} < -3.6$) and C-rich phases, $\tau_{\rm M}$ and $\tau_{\rm C}$, as a function of the stellar mass, for all metallicities considered here. It should be noted that these results are derived from the calibration of our TP-AGB tracks, which will be discussed in Sect. 4. Moreover, the TP-AGB lifetimes displayed in Fig. 22 account also for the last evolutionary stages characterised by the superwind mass-loss rates, i.e. the contribution from the dust-enshrouded, optically-obscured evolution is included in the computation of τ.

The termination of the TP-AGB phase, hence its duration, is determined by all those factors that concur to make the star lose its envelope. Clearly the main agent is mass loss by stellar winds, (and its complex dependence on basic stellar parameters like luminosity, effective temperature, chemical composition, pulsation, dust formation, etc.), but a certain role is also played by the rate of outward advancement by the H-burning shell that reduces the envelope mass from inside (and its dependence on factors like the metal content, and the occurrence of the third dredge-up and HBB). Actually it is worth mentioning that for $Z \leq 0.004$ low-mass TP-AGB models, say with $M \leq 0.7\,M_\odot$, never reach superwind mass-loss rates so that they leave the AGB because their envelope is eaten by the growth of the H-exhausted core.

The behaviour with metallicity of $\tau_{\rm M}$ at a given mass, displayed in the left panel of Fig. 22, depends on whether or not a TP-AGB model undergoes the third dredge-up. Lower-mass models that keep C/O < 1 up to the end of the AGB tend to have longer $\tau_{\rm M}$ at decreasing metallicity because of the lower rates of mass loss and/or core-mass growth.

In models of higher mass, which experience the third dredge-up, $\tau_{\rm M}$ is crucially affected by this latter process – which determines the stage at which the surface C/O > 1 – while it is essentially independent of the adopted mass-loss prescription. For these models the resulting trend of $\tau_{\rm M}$ is controlled by the mass and metallicity dependence of the main two dredge-up parameters, λ and $M_{\rm c}^{\rm min}$.

As we see there is a general tendency to have shorter $\tau_{\rm M}$ at decreasing metallicity because of the earlier onset and greater efficiency of the dredge-up at lower Z. It is interesting to note

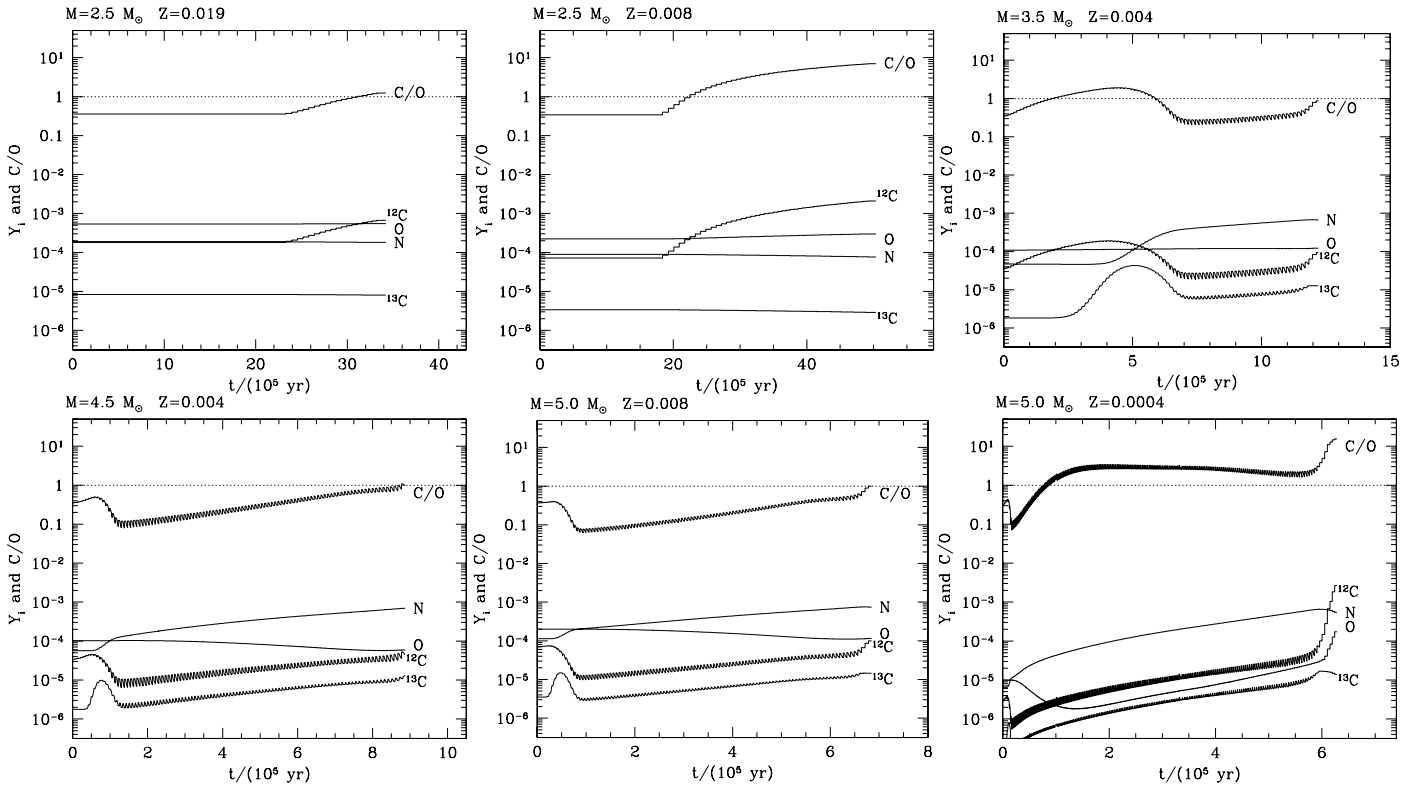

Fig. 21. Evolution of surface CNO abundances (in mole gr^{-1}) and C/O ratio during the TP-AGB phase of a few models with various initial masses and metallicities.

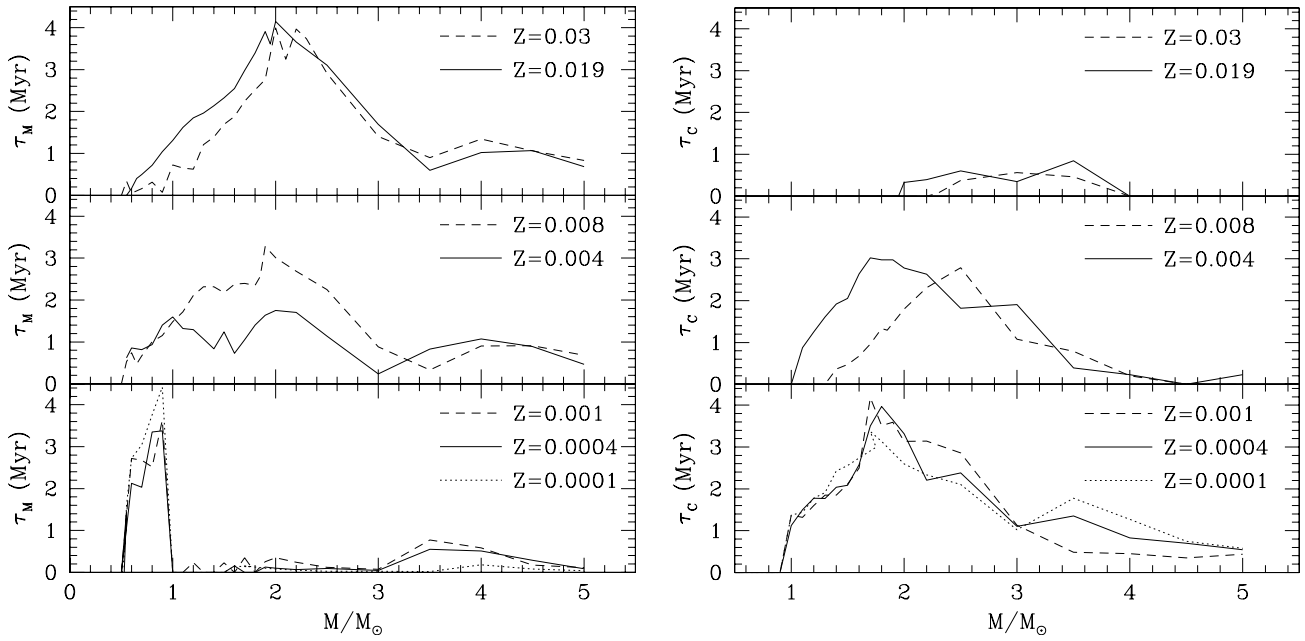

Fig. 22. Predicted duration of the phases spent by TP-AGB models as M-type stars ($\tau_{\rm M}$: *left panels*) and C-type stars ($\tau_{\rm C}$: *right panels*), as a function of both stellar mass and metallicity. For the sake of comparison with observations we consider stellar models with luminosities higher than $\log L/L_{\odot} = 3.33$, i.e., brighter than the RGB-tip at $M_{\rm bol} = -3.6$.

that for $Z \gtrsim 0.008$ the $\tau_{\rm M}(M_{\rm i})$ curve displays a peak at about $M_{\rm i} \simeq 1.9{-}2.2\,M_{\odot}$. This finding is to be at least partly ascribed to the relation $M_{\rm c,1TP}(M)$ at the first thermal pulse, which presents a minimum at these stellar masses, so that a relatively large growth of the core mass is required before the $M_{\rm c}^{\rm min}$ is attained. As we discuss in Sect. 4.2, this feature agrees with the observed maximum of M-type star counts in the Magellanic Clouds' clusters.

Concerning $\tau_{\rm C}$, shown in the right panel of Fig. 22, we note that the mean trend with metallicity is reversed compared to $\tau_{\rm M}$; i.e. the C-rich phase is expected to last longer at decreasing metallicity. For instance at $M_{\rm i} = 2.5\,M_{\odot}$, $\tau_{\rm C}$ passes from 0.6 Myr for $Z = 0.019$ to 2.8 Myr for $Z = 0.008$. However, we also see that moving to very low Z, $\tau_{\rm C}$ does not increase drastically; rather on average it stays almost invariant, e.g., $\tau_{\rm C} \sim 2.4$ Myr for

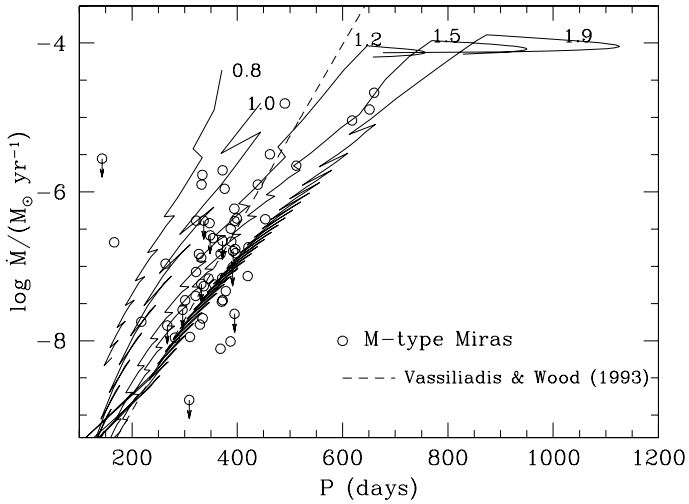

Fig. 23. Mass-loss rate versus period for O-rich Mira variables. Observed data (circles) correspond to Galactic M-type Miras (Le Bertre & Winters 1998; Groenewegen et al. 1999). For the sake of comparison we show the semi-empirical relation for Miras proposed by Vassiliadis & Wood (1993; dashed line), together with the theoretical predictions for evolving O-rich TP-AGB models with $Z = 0.019$ and various initial masses, based on Bowen & Willson (1991) wind models.

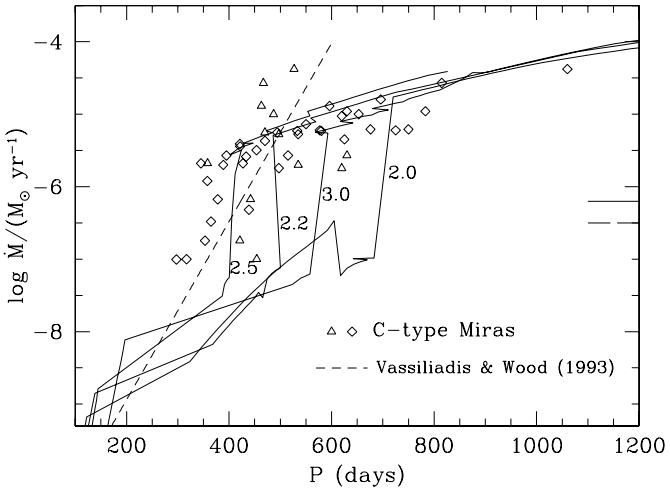

Fig. 24. Mass-loss rate versus period for C-rich Mira variables. Observed data correspond to Galactic C-rich Miras from Groenewegen et al. (1998; squares), and Schöier & Olofsson (2001; triangles). For the sake of comparison we show the semi-empirical relation for Miras proposed by Vassiliadis & Wood (1993; dashed line), together with the theoretical predictions for evolving C-rich TP-AGB models with $Z = 0.019$ and various initial mass, based on Wachter et al. (2002) wind models.

$Z = 0.0004$. This is the net result of the interplay between mass loss and dredge-up through their dependence on metallicity.

3.5. Mass-loss rates, periods and luminosities of variable AGB stars

The use of theoretically-derived mass-loss rates constitutes a major change with respect to our previous works. Leaving a detailed discussion of this subject to a future paper, below we simply illustrate the implications of our present choice.

Figure 23 compares a few of our O-rich TP-AGB tracks of solar composition with the data for Galactic M-type Miras in the $\dot{M}$–P diagram. It can be noticed that the models reproduce the ranges of mass-loss rates and periods covered by the data well. In particular, the significant dispersion in $\dot{M}$ at given P exhibited by the Miras is accounted for by the models at varying mass. The observed spread cannot be obtained, instead, by applying, for instance, the Vassiliadis & Wood (1993) formalism that gives $\dot{M}$ as a sole function of P. Moreover, the onset of the superwind phase (with $\dot{M} \approx 10^{-5}$–$10^{-4}\,M_\odot\,\mathrm{yr}^{-1}$) is naturally predicted with the adopted scheme and allows the reproduction of the OH/IR data over a wide period range.

Similar comments can be made about the mass-loss rates in the C-rich phase, as illustrated in Fig. 24. What is more evident in this case is that models reproduce the plateau at $\dot{M} \approx 10^{-5}\,M_\odot\,\mathrm{yr}^{-1}$ in $\dot{M}$, corresponding to the superwind phase of C-type stars.

Extensive observations of Miras in the LMC have shown that these variables populate a well-defined period-luminosity (P–L) relation (e.g., Feast et al. 1989; Hughes & Wood 1990; MACHO survey), as displayed in Fig. 25 for both oxygen- and carbon-rich objects.

The TP-AGB evolutionary tracks at varying initial mass and with $Z = 0.019$ and $Z = 0.008$ are superimposed for the sake of comparison. According to the assumed description of pulsation (see Sect. 2.7), tracks split into two bundles in the P–L diagram, the one at shorter P corresponding to the FOM, and the other at longer P corresponding to the FM. Clearly this latter group turns out to be consistent with the observed location of Miras, supporting the indication that these variables are pulsating in the fundamental mode.

A detailed investigation of the several variability sequences, in addition to that of Miras, that populate the P–L diagram (e.g. Wood et al. 1999) are beyond the scope of the present study. To this aim it is necessary to perform population synthesis simulations that couple updated TP-AGB tracks with LPV models for different pulsation modes. This kind of analysis is underway.

3.6. The initial-final mass relation

The initial-final mass relation (IFMR) is affected by the competition between core growth by shell burning and core reduction by third dredge-up events, the final result depending on the termination of the AGB evolution by stellar winds. Since dredge-up is more efficient at higher masses and lower metallicities, one may naively expect that this competition will favour flatter IFMR at lower metallicities. Actually, this may not happen because the IFMR also carries a strong imprinting of the core mass at the first thermal pulse, which is in general greater at lower metallicities (see e.g., Fig. 1 in Girardi & Bertelli 1998). Moreover, the higher efficiency of HBB at lower metallicities may reduce the TP-AGB lifetime in such a way that less time is left for the core mass to significantly change along the TP-AGB. Finally, the IFMR is modulated by the TP-AGB lifetimes, the complex dependence of which as a function of mass and metallicity is shown in Fig. 22. Therefore, the actual shape of the IFMR and its variation with metallicity depends on several parameters, and it cannot be easily predicted via simple reasonings.

Figure 26 shows the IFMR as predicted by current models of various metallicities, compared to recent observational data for white dwarfs in binary systems and open clusters. In general, both the cluster ages and white dwarf progenitor masses have been estimated (or checked) by using tracks and isochrones from Girardi et al. (2000), so that the plot should not contain inconsistencies associated to the use of different prescriptions for

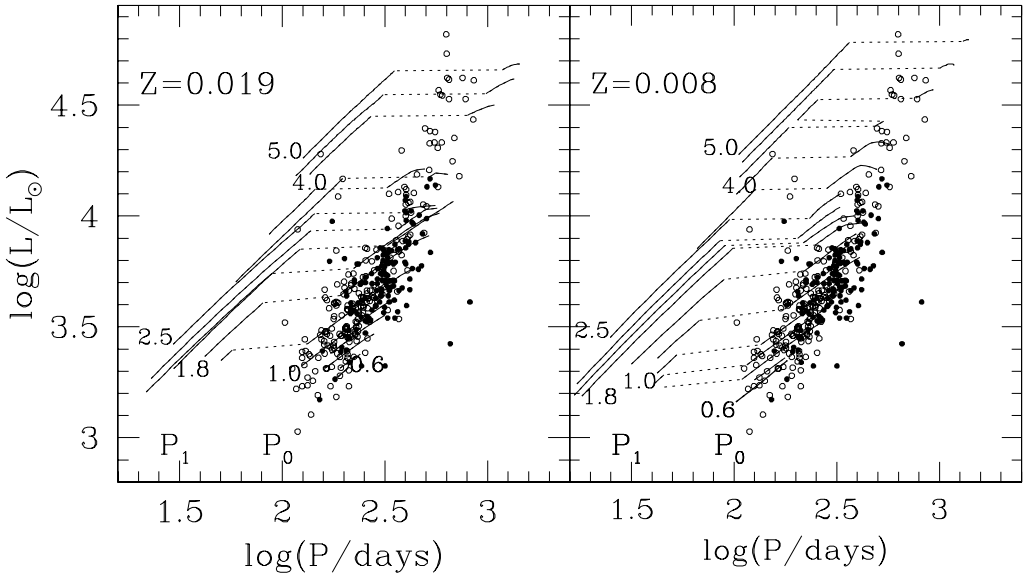

Fig. 25. Period-luminosity relation of Mira variables in the LMC. Observed data correspond to M-type (empty circles) and C-type Miras (filled circles) LMC (Feast et al. 1989; Hughes & Wood 1990), assuming a distance modulus μ_0 = 18.5. Lines show the theoretical tracks described by TP-AGB models for two choices of metallicity and with initial stellar masses ranging from 0.6 to 5.0 $M_\odot$ (a few values are indicated). It is assumed that pulsation occurs initially in the FOM (P_1 sequence) and then it switches to the FM (P_0 sequence). See text for more explanation.

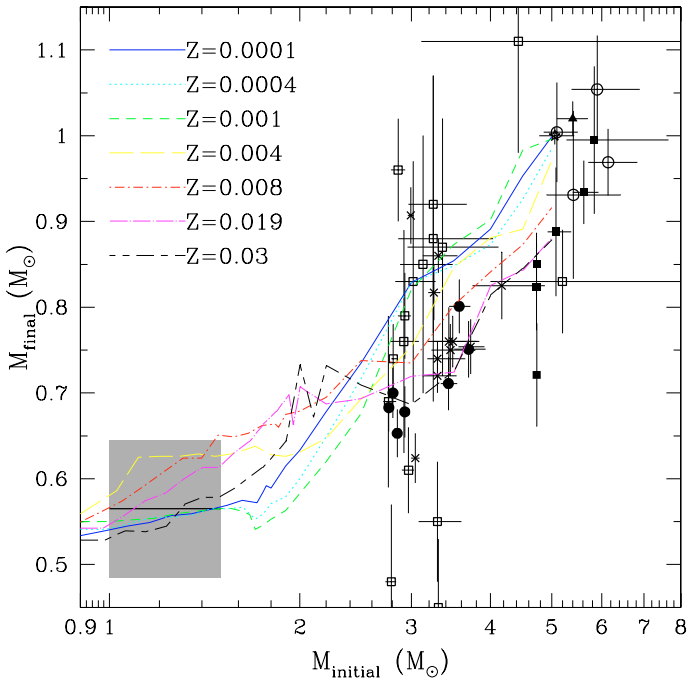

Fig. 26. The initial–final mass relation from our models (lines) for several metallicities, together with the empirical data for white dwarfs in open clusters and binary systems: the Hyades (full circles, Claver et al. 2001), M 37 (open squares, Kalirai et al. 2005), Praesepe (crosses, Claver et al. 2001, and Dobbie et al. 2006), M 35 (full squares, Williams et al. 2004), Sirius B (star, Liebert et al. 2005a), Pleiades (full triangle, Dobbie et al. 2006), and NGC 2516 (open circles, Ferrario et al. 2005). The gray area indicates the position (mean and 1σ) of the primary mass peak of field white dwarfs as measured by Liebert et al. (2005b), which we indicate associated to the 1.0–1.5 $M_\odot$ interval.

convective overshooting. It is worth noticing that:

1) The predicted IFMR have a significant dependence on metallicity. For a given initial mass the allowed range of final masses is about 0.1 $M_\odot$ wide. The dependence is such that the IFMR is steeper at low metallicities. Although the final mass generally increases with the initial mass, there are limited mass ranges in which this trend is reversed (e.g., for the Z = 0.03 tracks in the 2.2−3 $M_\odot$ interval), as well as small track-to-track variations that arise from the complex interplay between the evolutionary parameters involved.
2) The data seems to be too dispersed to allow a firm testing of the model predictions, but this dispersion strongly depends on the data for the M 37 cluster (from Kalirai et al. 2005), which – apart from a few low-mass outlyers – lie systematically above the mean relation drawn by the remaining objects. As noted by Dobbie et al. (2006), the mass determinations of M 37 white dwarfs may still change considerably since its initial metallicity is not well-determined. Excluding the M 37 white dwarfs, the IMFR is well-defined for the complete range of $M_\mathrm{i} > 2.5\ M_\odot$. On the other hand, good-quality data covering the 1.5−2.5 $M_\odot$ mass range are presently not available. Notice that we have represented the <1.5 $M_\odot$ mass range by field white dwarfs, whose initial mass is not directly measured.
3) If we do not consider the M 37 white dwarfs, the comparison between the data and the model IFMRs for close-to-solar metallicities (the Z = 0.019 and 0.03 curves) turns out to be very satisfactory over the entire $M_\mathrm{i} < 5\ M_\odot$ mass range. It seems advisable, however, to extend the TP-AGB model computations to slightly higher initial masses, in order to explain the few points observed at $M_\mathrm{i} > 5.5\ M_\odot$. In this regard, more recent evolutionary tracks from Padova (Bertelli et al., in preparation) suggest that the highest mass for entering in the TP-AGB phase, using the Girardi et al. (2000) prescription for overshooting, is located somewhere between 5.5 and 6 $M_\odot$, rather than equal to the 5 $M_\odot$ mentioned by Girardi et al.

Future works in this series will improve on this point and present detailed comparisons with the mass distribution of field white dwarfs.

4. Calibration of TP-AGB model parameters

In this section, we first briefly present the set of Magellanic Cloud data used to constrain the TP-AGB model parameters, together with the methods employed to simulate the data starting from the TP-AGB tracks. The calibration process is fully described in the Appendix.

We note that previous sets of calibrated TP-AGB models (e.g., Groenewegen & de Jong 1993; Marigo et al. 1999) have

used the C-star luminosity functions in the Magellanic Clusters as, basically, the only observational constraint. To the CSLFs, we now add the C- and M-type lifetimes as described below. Previous works have also adopted descriptions that are too simple for the star formation rate (SFR) and age-metallicity relations (AMR) of both galaxies, such as a constant SFR and a constant metallicity with varying age. We now improve upon this approach by adopting SFR and AMR independently derived by other authors to simulate the data.

4.1. Carbon-star luminosity functions in the Magellanic Clouds

The CSLF in several Local Group galaxies have been reviewed and compared by Groenewegen (2002; see also Groenewegen 1999), who kindly provided us with his latest data files for both Magellanic Clouds. The observed CSLF in the LMC makes use of the Costa & Frogel (1996) $m_{\rm bol}$ data, which refers to 895 carbon stars among the original sample of 1035 stars distributed in 52 LMC fields over an area of $8^\circ \times 8^\circ$. This sample of carbon stars can be considered almost complete and not limited by apparent magnitude, since the faintest carbon stars are at least 2 mag brighter ($I \sim 15$) than the faint limit of detection ($I \sim 17$) of the original surveys (Blanco et al. 1980; Blanco & McCarthy 1983). The fraction of optically-obscured carbon stars, which would have been missed in the survey because of dust obscuration, has been estimated to be lower than 3% for $M_{\rm bol} < -6$ (Groenewegen & de Jong 1993). The conversion from the photometry to bolometric magnitudes has been performed by Costa & Frogel (1996), who mention a mean error on the evaluation of $m_{\rm bol}$ of approximately 0.34 mag. Finally, the absolute bolometric magnitudes, $M_{\rm bol}$, are then obtained by adopting a distance modulus of $\mu_0 = 18.5$ for the LMC. The resulting CSLF extends approximately from $M_{\rm bol} = -3$ up to $M_{\rm bol} = -6.5$, with the peak located at around $M_{\rm bol} = -4.875$.

The observed CSLF in the SMC has been derived by Groenewegen (1997) from a sample of 1636 stars observed by Rebeirot et al. (1993), and adopting bolometric correction by Westerlund et al. (1986). The adopted distance modulus for the SMC is $\mu_0 = 19.0$. The first bin of this CSLF contains all stars fainter than $M_{\rm bol} = -2.5$, which comprise less than 3% of the total sample of SMC carbon stars. Their intrinsic magnitudes can be as low as $M_{\rm bol} = -1.8$, as found by Westerlund et al. (1995). The formation of carbon stars at such low luminosities can hardly be understood as the result of the third dredge-up in single AGB stars, and most likely they arise from the transfer of mass in close binary systems (see e.g. de Kool & Green 1995; Frantsman 1997). These low-luminosity carbon stars will not be considered in this work, since we are dealing with single star evolution. For all practical comparisons, we will consider the CSLF in the SMC as extending down to $M_{\rm bol} = -2.5$. The resulting CSLF extends up to $M_{\rm bol} = -6.5$, with the peak located at $M_{\rm bol} = -4.375$.

Recently Guandalini et al. (2006) have claimed that bolometric corrections for C stars are systematically underestimed because neglecting the flux in the mid-IR and suggested that accounting for this flux would imply overall much brighter CSLFs. Although their arguments are unimpeachable, it is worth noticing that their study is based on a sample of C stars in the Milky Way selected to have mid-IR photometry. Such a sample is much more prone to containing IR-bright objects – of cool temperatures and undergoing significant mass loss and dust obscuration – than samples extracted from optical to near-IR surveys. This is also indicated by the fact that the majority of their stars have $J - K > 2.0$ (see their Fig. 7), which corresponds to the colour interval of C stars strongly affected by circumstellar dust. The bulk of C stars observed in the Magellanic Clouds, instead, have $J - K$ between 1.2 and 2.0 (e.g. Nikolaev & Weimberg 2000), and it is expected to be overall much hotter and cleaner from dust than the Guandalini et al. (2006) sample. Moreover, we note that both observations (van Loon et al. 2005) and population synthesis models based on the present evolutionary tracks (Marigo et al., in prep.) agree in estimating as ≈10−20% the fraction of dust-enshrouded C-stars in the Magellanic Clouds, i.e. the bulk of their C-star population consists of optically-visible objects with just mild mid-IR emission. Therefore, we consider it unlikely that the consideration of the mid-IR flux would significantly affect the CSLFs here discussed.

4.2. TP-AGB lifetimes: M- and C-type phases

Limits to the lifetimes of the M- and C-type TP-AGB phase have been recently derived by Girardi & Marigo (2007), using available data for C and M giants with $M_{\rm bol} < -3.6$ in Magellanic Cloud clusters (Frogel et al. 1990), together with the clusters' integrated V-band luminosities (from Bica et al. 1996; and van den Bergh 1981). They essentially find the C-star phase has a duration between 2 and 3 Myr for stars in the mass range from ∼1.5 to 2.8 $M_\odot$, with some indication that the peak of C-star lifetime shifts to lower masses as we move from LMC to SMC metallicities. The M-giant lifetimes is found to peak at ∼2 $M_\odot$ in the LMC, with a maximum value of about 4 Myr, whereas in the SMC their lifetimes are poorly constrained by the data. Therefore, in the following we will only deal with the C-star lifetimes for both LMC and SMC and with the M-star lifetime above $M_{\rm bol} < -3.6$ for the LMC.

Our aim is to obtain theoretical TP-AGB lifetimes that fit the Girardi & Marigo (2007) values, within the 67% confidence level of the observations (1σ for the most populated age bins), over the complete 0.8−5 $M_\odot$ interval for the formation of TP-AGB stars. Although this 67% confidence level interval may look quite ample, they constitute very useful constraints. In fact, Girardi & Marigo (2007) show that many TP-AGB models in the literature do present C-star lifetimes that are too short, and/or fail to reproduce the observed trends of the lifetimes with the initial mass.

4.3. Modelling the CSLF and lifetimes

In order to simulate the CSLF starting from TP-AGB tracks, we follow a complex but well-tested procedure, which is somewhat more elaborate than the one described in Marigo et al. (1999). First, the tracks on their quiescent phases of evolution are assembled, together with the previous evolution given by Girardi et al. (2000) tracks. Theoretical isochrones are then constructed via interpolation for any intermediate value of age and metallicity (Marigo & Girardi, in preparation). The isochrone section corresponding to the C-star phase – with their quiescent luminosities – is then isolated; for each point on it, the pulse-cycle luminosity variations are reconstructed using Wagenhuber & Groenewegen (1998) formula, together with basic stellar parameters like the metallicity and core mass. This allows us to attribute the complete luminosity probability distribution function to each quiescent point in the isochrone and hence to construct the CSLF for each single-burst stellar population via integration along the corresponding isochrone. Then, we integrate over population age,

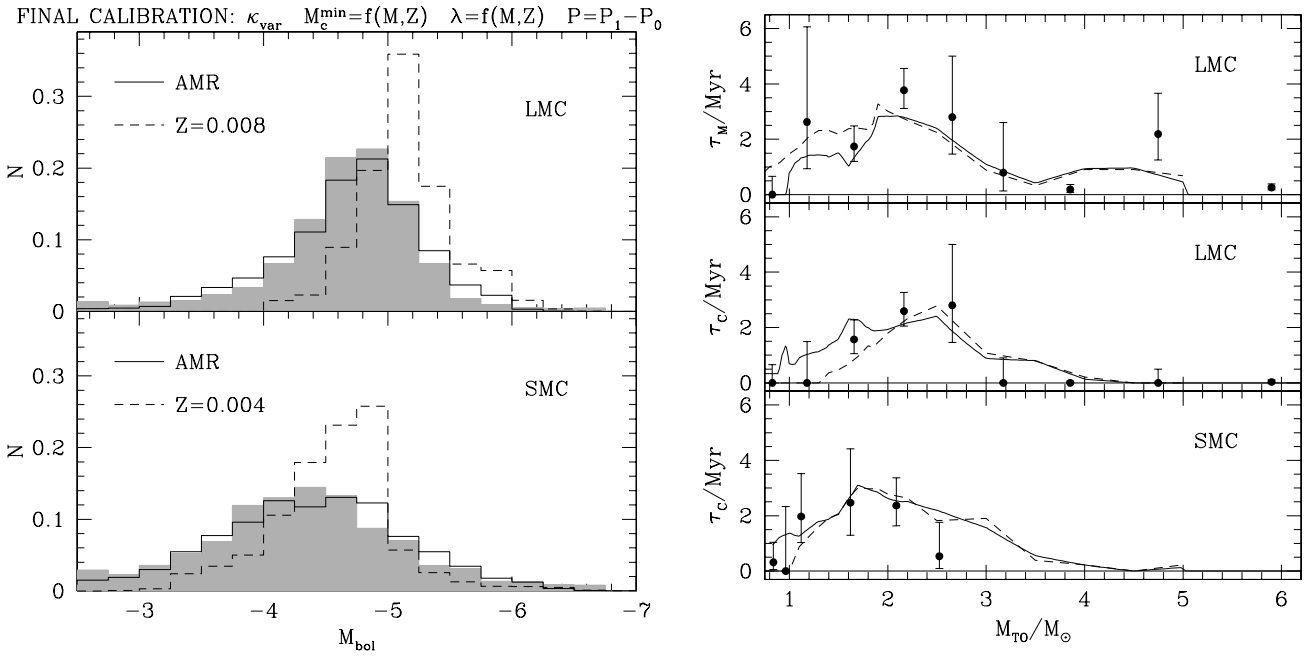

Fig. 27. The final model calibration. *Left panels*: the observed C star luminosity functions (CSLF) in the Magellanic Clouds (Groenewegen 2002; shaded areas), as compared to the synthetic ones derived from present models. *Right panels*: the observed C- and M-type lifetimes in the Magellanic Clouds (Girardi & Marigo 2007), as compared to the same models.

weighting each age by its relative SFR and using the AMR to select the right metallicity value at each age.

As for the LMC, we have adopted the SFR determined by Holtzman et al. (1999) in an outer field close to Hodge 4, using deep HST data. For the SMC, we used the global SFR as determined by Harris & Zaritsky (2004) from the Magellanic Clouds Photometric Survey. In both cases, the SFR were reconstructed using objective algorithms of CMD fitting. Their results were mostly determined by the star counts in the main phases of pre-AGB evolution (main sequence, subgiant and red giant branches, red clump) and, important for us, are unlikely to be sensitive to the (relatively very few) TP-AGB stars present in their data.

We adopted the AMRs from the "bursting models" of chemical evolution for the LMC and SMC by Pagel & Tautvaisiene (1998). These relations, although theoretical in nature, were designed to reproduce the age-metallicity data for star clusters in both Clouds.

The TP-AGB lifetimes in the C- and M-type phases were derived directly from the tracks, first identifying the turn-off mass and population age of each TP-AGB track, then interpolating the turn-off mass and TP-AGB lifetimes for each metallicity–age value given in the AMR. As a result, we derived the expected TP-AGB lifetimes (above $M_{\rm bol} = -3.6$) as a function of turn-off mass, that can be directly compared to the data tabulated by Girardi & Marigo (2007).

We notice that, with the present prescriptions for the mass-loss rates, the superwind phase (with $\dot{M} \gtrsim 5.6 \times 10^{-7}\, M_\odot\, {\rm yr}^{-1}$) for which the stars are likely to be optically obscured, lasts less than 20 percent of the TP-AGB lifetime for all tracks with $Z \lesssim 0.008$. For models with $1.5 \lesssim (M/M_\odot) \lesssim 2.5$ of such metallicities, which enter the superwind phase as C stars and are the most relevant for the comparison with MC data, the superwind phase typically lasts less than 15 percent of the C-star lifetime. These numbers roughly agree with those derived from observations in the MCs (van Loon et al. 2005). A detailed analysis of this point is left to subsequent papers in this series. We advance however, that the neglection of objects that are likely to be optically-obscured in the theoretical CSLFs and lifetimes, as we verified, would not significantly affect our calibration iter. The Appendix summarises the calibration iter, starting from the past calibration of Marigo et al. (1999) and arriving at the final result depicted in Fig. 27.

4.4. Implications from the calibration

The calibration sequence described in the Appendix yields a number of interesting and useful indications, namely:

1) The combined use of both CSLFs and stellar lifetimes in the Magellanic Clouds as calibrating observables strengthens the reliability of the underlying TP-AGB description. In fact, we find that sets of models, consistent with the data for the C- and M-star lifetimes, may instead not reproduce the corresponding luminosity functions and vice versa.
2) Due to the pronounced metallicity dependence of the third dredge-up, any theoretical investigation of the C-stars' populations should account for the history of chemical enrichment in the host galaxies, then relaxing the much too simple assumption of constant metallicity. Indeed, the simultaneous reproduction of the CSLFs in both Magellanic Clouds provides a strong indication in this respect, as we see in Fig. 27 when comparing the results for Z = const. to those obtained including proper AMRs in the simulated galaxies. In particular, we see that the excess of bright C stars and the deficiency of fainter objects, predicted while assuming Z = const., are removed when accounting for the metallicity-dependence of the third dredge-up. This means that the extent of the long-standing theoretical difficulty in producing faint carbon stars, known as 'the carbon star mystery" since Iben (1981), could actually be less important than so far believed, just because of a metallicity mismatch in the comparison between observations and predictions. Moreover, the fact that the populations of C stars in the two galaxies share a common metallicity

range, say around $Z = 0.004$, should make our metallicity calibration for the third dredge-up more constrained.

3) The peak of the M-star lifetimes in the LMC clusters (limiting to stars brighter than the RGB-tip) is recovered only assuming that the third dredge-up in stars with $M_{\rm i} \sim 1.7{-}2.5\ M_{\odot}$ and $Z \approx 0.008$ does not take place as soon as they enter the TP-AGB phase, but somewhat later. The $M_{\rm c}^{\rm min}(M,Z)$ formalism derived by K02 turns out to be consistent with this indication. In this way, we alleviate the problem of underestimating the M-star populations that affects the simulations presented in Cioni et al. (2006a,b).
4) The decreasing lifetimes of C stars with $M_{\rm i} > 2.5\ M_{\odot}$ seen in both Magellanic Clouds is due to the concomitant effects of their brighter luminosities – that favour the earlier onset of the superwind – and, in models of larger masses (with $M_{\rm i} \gtrsim 4.0\ M_{\odot}$), of the occurrence of HBB – that may later reconvert a C star into an M star, or even prevent the transition to the C-star domain.

5. Final remarks

The set of TP-AGB evolutionary tracks presented in this paper constitutes a very useful database for population studies, due to several distiguishing features.

1) We have used updated ingredients and improved treatment of some key physical processes in the synthetic AGB code, as extensively discussed in Sects. 2 and 3. The most important updating is no doubt the use of variable molecular opacities instead of the scaled-solar tables still used in complete AGB models. Previous sets of models using these opacities have already been used (Marigo 2002; Marigo et al. 2003; Cioni et al. 2006a,b) and distributed by us (see Cioni et al. 2006a and `http://pleiadi.oapd.inaf.it`), but this is the first time *calibrated* TP-AGB tracks using this approach have been released.
2) The present model calibration (Sect. 4) is based not only on the reproduction of the CSLFs in both Magellanic Clouds, but also on the data for C- and M-star counts in Magellanic Cloud clusters. It means that present models have the right luminosities for the TP-AGB phase (as ensured by the CSLF calibration), and also that they present, as far as possible, the right lifetimes at Magellanic Cloud metallicities. The contribution of any post-MS evolutionary stage to the integrated light of a single-burst stellar population is proportional to the product of luminosity and lifetime – also known as the *nuclear fuel* in the context of the fuel consumption theorem (Renzini & Buzzoni 1986). Therefore, evolutionary population synthesis models that use the present TP-AGB tracks will present the right contribution of TP-AGB stars to the integrated light at Magellanic Clouds metallicities and, hopefully, also a good description of the way this contribution varies with metallicity.
3) The present tracks nicely complement the sets of low- and intermediate-mass models of Girardi et al. (2000) and Girardi (2002, unpublished), which deal with the evolution from the zero-age main sequence up to the first thermal pulse. In fact, when coupling both sets of tracks together one will find no discontinuities in quantities like the core mass and chemical surface composition. Discontinuities in the HR diagram may appear due to the use of slightly different low-temperature opacities; however, we checked that they are tiny and certainly much less serious than those that occur when amalgamating tracks from different sources. Therefore, one has the possibility of building consistent tracks all the way from the ZAMS to the end of the TP-AGB. Of course, this sequence can also be extended with any suitable set of post-AGB tracks (e.g., Vassiliadis & Wood 1994), so as to cover the subsequent evolution up to the WD stages.
4) We made a first attempt to describe the switching of pulsation modes between the first overtone and fundamental one along the TP-AGB evolution. These changes have some consequence in terms of the history of mass loss and open new possibilities for better calibrating TP-AGB tracks by means of comparison with the extensive variability surveys in the Magellanic Clouds.

Forthcoming papers will present extensive and ready-to-use theoretical isochrones and chemical yields from these tracks, as well as several population synthesis applications.

Acknowledgements. We thank the anonymous referee and Martin Groenewegen for their useful remarks. This study was partially supported by the University of Padova (Progetto di Ricerca di Ateneo CPDA052212).

References

Alexander, D. R., & Ferguson, J. W. 1994, ApJ, 437, 879
Alongi, M., Bertelli, G., Bressan, A., Chiosi, C., Fagotto, F., et al. 1993, A&AS, 97, 851
Battinelli, P., & Demers, S. 2005a, A&A, 434, 657
Battinelli, P., & Demers, S. 2005b, A&A, 442, 159
Bedijn, P. J. 1988, A&A, 205, 105
Bergeat, J., Knapik, A., & Rutily, B. 2001, A&A, 369, 178
Bica, E., Clariá, J. J., Dottori, H., Santos, J. F. C., Jr., & Piatti, A. E. 1996, ApJS, 102, 57
Blanco, V. M., & McCarthy, M. F. 1983,
Blanco, V. M., Blanco, B. M., & McCarthy, M. F. 1980, ApJ, 242, 938
Blum, R. D., Mould, J. R., Olsen, K. A., et al. 2006, AJ, 132, 2034
Boothroyd, A. I., & Sackmann, I.-J. 1988, ApJ, 328, 653
Bowen, G. H. 1988, ApJ, 329, 299
Bowen, G. H., & Willson, L. A. 1991, ApJ, 375, L53
Cioni, M.-R., Habing, H. J., Loup, C., Groenewegen, M. A. T., Epchtein, N., & the DENIS Consortium 1999, IAUS, 192, 65
Cioni, M.-R. L., Blommaert, J. A. D. L., Groenewegen, M. A. T., et al. 2003, A&A, 406, 51
Cioni, M.-R. L., Girardi, L., Marigo, P., & Habing, H. J. 2006a, A&A, 448, 77
Cioni, M.-R. L., Girardi, L., Marigo, P., & Habing, H. J. 2006b, A&A, 452, 195
Claver, C. F., Liebert, J., Bergeron P., & Koester, D. 2001, ApJ, 563, 987
Costa, E., & Frogel, J. A. 1996, AJ, 112, 2607
de Kool, M., & Green, P. J. 1995, ApJ, 449, 236
Dobbie, P. D., Napiwotzki, R., & Burleigh, M. R., et al. 2006, MNRAS, 369, 383
Feast, M. W., Glass, I. S., Whitelock, P. A., & Catchpole, R. M. 1989, MNRAS, 241, 375
Ferrario, L., Wickramasinghe, D., Liebert, J., & Williams, K. A. 2005, MNRAS, 361, 1131
Fleischer, A. J., Gauger, A., & Sedlmayr, E. 1992, A&A, 266, 321
Fox, M. W., & Wood, P. R. 1982, ApJ, 259, 198
Frantsman, J. 1997, A&A, 319, 511
Frost, C. A., Cannon, R. C., Lattanzio, J. C., Wood, P. R., & Forestini, M. 1998, A&A, 332, L17
Fraser, O. J., Hawley, S. L., Cook, K. H., & Keller, S. C. 2005, ApJ, 129, 768
Frogel, J. A., Mould, J., & Blanco, V. M. 1990, ApJ, 352, 96
Girardi, L., & Bertelli, G. 1998, MNRAS, 300, 533
Girardi, L., & Marigo, P. 2007, A&A, 462, 237
Girardi, L., Bressan, A., Bertelli, G., & Chiosi, C. 2000, A&AS, 141, 371
Groenewegen, M. A. T. 1997, Ap&SS, 255, 379
Groenewegen, M. A. T. 1999, IAUS, 191, 535
Groenewegen, M. A. T. 2002 [arXiv:astro-ph/0208449]
Groenewegen, M. A. T. 2004, A&A, 425, 595
Groenewegen, M. A. T., & de Jong, T. 1993, A&A, 267, 410
Groenewegen, M. A. T., & de Jong, T. 1994, A&A, 283, 463
Groenewegen, M. A. T., & Marigo, P. 2003, in Asymptotic Giant Branch Stars, Chap. 3, ed. H. J. Habing, & Hans Olofsson (Astronomy and Astrophysics Library)
Groenewegen, M. A. T., Whitelock, P. A., Smith, C. H., & Kerschbaum, F. 1998, MNRAS, 293, 18

Groenewegen, M. A. T., Baas, F., Blommaert, J. A. D. L., et al. 1999, A&AS, 140, 197
Harris, J., & Zaritsky, D. 2004, AJ, 127, 1531
Herwig, F. 2005, ARA&A, 43, 435
Höfner, S., Sandin, C., Aringer, B., et al. 2003, IAUS, 210, 353
Holtzman, J. A., Gallagher, J. S., III, Cole, A. A., et al. 1999, AJ, 118, 2262
Hughes, S. M. C., & Wood, P. R. 1990, AJ, 99, 784
Iglesias, C. A., & Rogers, F. J. 1993, ApJ, 412, 752
Izzard, R. G., Tout, C. A., Karakas, A. I., & Pols, O. R. 2004, MNRAS, 350, 407 (I04)
Kalirai, J. S., Richer, H. B., Reitzel, D., et al. 2005, ApJ, 618, L123
Karakas, A. I., Lattanzio, J. C., & Pols, O. R. 2002, PASA, 19, 515 (K02)
Lattanzio, J. C., & Wood, P. P. 2003, in Asymptotic Giant Branch Stars, Chap. 2, ed. H. J. Habing, & H. Olofsson (Astronomy and Astrophysics Library)
Le Bertre, T. 1997, A&A, 324, 1059
Le Bertre, T., & Winters, J. M. 1998, A&A, 334, 173
Liebert, J., Young, P. A., Arnett, D., Holberg, J. B., & Williams, K. A. 2005a, ApJ, 630, L69
Liebert, J., Bergeron, P., & Holberg, J. B. 2005b, ApJS, 156, 47
Loup, C., Josselin, E., Cioni, M.-R., et al. 1999, IAUS, 191, 561
Marigo, P. 2001, A&A, 370, 194
Marigo, P. 2002, A&A, 387, 507
Marigo, P., Bressan, A., & Chiosi, C. 1996, A&A, 313, 545
Marigo, P., Bressan, A., & Chiosi, C. 1998, A&A, 331, 564
Marigo, P., Girardi, L., & Bressan, A. 1999, A&A, 344, 123
Marigo, P., Girardi, L., & Chiosi, C. 2003, A&A, 403, 225
Mouhcine, M., & Lançon, A. 2002, A&A, 393, 149
Nikolaev, S., & Weinberg, M. D. 2000, ApJ, 542, 804
Olofsson, H., González Delgado, D., Kerschbaum, F., & Schöier, F. L. 2002, A&A, 391, 1053
Ostlie, D. A., & Cox, A. N. 1986, ApJ, 311, 864
Pagel, B. E. J., & Tautvaisiene, G. 1998, MNRAS, 299, 535
Rebeirot, E., Azzopardi, M., & Westerlund, B. E. 1993, A&AS, 97, 603
Renzini, A., & Buzzoni, A. 1986, in Spectral Evolution of Galaxies, ed. C. Chiosi, & A. Renzini (Dordrecht, Reidel), 195
Romano, D. Matteucci, F., Ventura, P., & D'Antona, F. 2004, A&A, 374, 646
Ita, Y., Tanabé, T., Matsunaga, N., et al. 2004, MNRAS, 353, 705
Schöier, F. L., & Olofsson, H. 2001, A&A, 368, 969
Schröder, K.-P., Winters, J. M., & Sedlmayr, E. 1999, A&A, 349, 898
Sedlmayr, E., & Winters, J. M. 1997, in Stellar Evolution, ed. R. T. Rood, & A. Renzini (Cambridge University Press, UK), 169
Stancliffe, R. J., Izzard, R. G., & Tout, C. A. 2005, MNRAS, 356, L1
Soszynski, I., Udalski, A., Kubiak, M., et al. 2005, AcA, 55, 331
van den Bergh, S. 1981, A&AS, 46, 79
van Loon, J. T., Zijlstra, A. A., Whitelock, P. A., et al. 1997, A&A, 325, 585
van Loon, J. T., Marshall, J. R., Zijlstra, A. A., et al. 2005, A&A, 442, 597
Vassiliadis, E., & Wood, P. R. 1993, ApJ, 413, 641
Vassiliadis, E., & Wood, P. R. 1994, ApJS, 92, 125
Ventura, P., D'Antona, F., & Mazzitelli, I. 2002, A&A, 393, 215
Wachter, A., Schröder, K.-P., Winters, J. M., Arndt, T. U., & Sedlmayr, E. 2002, A&A, 384, 452
Wagenhuber, J., & Tuchman, Y. 1996, A&A, 311, 509
Wagenhuber, J., & Groenewegen, M. A. T. 1998, A&A, 340, 183
Westerlund, B. E., Azzopardi, M., & Breysacher, J. 1986, A&AS, 65, 79
Westerlund, B. E., Azzopardi, M., Breysacher, J., & Rebeirot, E. 1995, A&A, 303, 107
Winters, J. M., Le Bertre, T., Jeong, K. S., Helling, Ch., & Sedlmayr, E. 2000, A&A, 361, 641
Winters, J. M., Le Bertre, T., Jeong, K. S., Nyman, L.-A., & Epchtein, N. 2003, A&A, 409, 715
Williams, K. A., Bolte, M., & Koester, D. 2004, ApJ, 615, L49
Willson 2000, ARA&A, 38, 573
Wood, P. R. 1990, in From Miras to planetary nebulae: Which path for stellar evolution?, Gif-sur-Yvette, France (Editions Frontières), 67
Wood, P. R., Bessell, M. S., & Fox, M. W. 1983, ApJ, 272, 99
Wood, P. R., Alcock, C., Allsman, R. A., et al. 1999, in Asymptotic Giant Branch Stars, IAUS, 191, 151
Ya'Ari, A., & Tuchman, Y. 1996, ApJ, 456, 350

Online Material

Appendix A: The model calibration

This section summarises the calibration iter, mainly involving the parameterised decription of the third dredge-up. We also discuss the strong influence played by other parameters, like the assumed pulsation mode on the mass-loss rates and the age-metallicity relation of the host galaxy.

The most relevant calibrating steps are illustrated through the sequence of panels from Figs. A.1 to 27, where labels indicate the main model assumptions, namely:

- molecular opacities, either fixed for solar-scaled mixtures, $\kappa_{\rm fix}$, or variable chemical composition, $\kappa_{\rm var}$;
- dredge-up efficiency λ;
- onset of the third dredge-up, determined by either the temperature $T_{\rm b}^{\rm dred}$ parameter, or the classical $M_{\rm c}^{\rm min}$ parameter.
- pulsation mode, either fundamental with $P = P_0$, or first overtone with $P = P_1$;
- metallicity of the simulated galaxy, either assumed constant over its entire history, Z = const., or made vary according to a specified age-metallicity relation, AMR.

Figure A.1 illustrates the results obtained with the same prescriptions for the third dredge-up as in our previous study (Marigo et al. 1999). The most significant difference between the two sets of models is the adoption in the present calculations of variable molecular opacities in place of those for solar-scaled mixtures. In both cases mass loss is treated with the aid the Vassiliadis & Wood (1993) formalism, always assuming FM pulsation ($P = P_0$).

We notice that the combination ($\log T_{\rm b}^{\rm dred} = 6.40, \lambda = 0.5$) now fails to reproduce the CSLF in the LMC – instead providing the best fit in the previous calibration by Marigo et al. (1999) – while it well recovers the C-star lifetimes in both Magellanic Clouds. A reasonable fit to the CSLF in the LMC is obtained with the ($\log T_{\rm b}^{\rm dred} = 6.45, \lambda = 0.5$) case, but the duration of the C-star phase as a function of $M_{\rm i}$ is somewhat underestimated. The ($\log T_{\rm b}^{\rm dred} = 6.50, \lambda = 0.5$) set of models yields poor results with respect to all observables. Finally, we should point out that all combinations of dredge-up parameters do not reproduce the CSLF in the SMC, and they substantially underestimate the duration of the M-star phase in the 1.8−3.0 $M_\odot$ range.

Figure A.2 is based on models calculated with exactly the same input parameters as Fig. A.1, except that pulsation is assumed to occur in the FOM. With the assumption $P = P_1$, the predicted CSLFs tend to populate brighter luminosities, as a consequence of the fact that shorter periods correspond to lower mass-loss rates, hence longer TP-AGB lifetimes. From this comparison with the observed data it turns out that (i) none of the ($T_{\rm b}^{\rm dred}, \lambda$) combinations leads to a satisfactory reproduction of the CSLFs; (ii) the C-star lifetimes are relatively well-recovered; (iii) the M-star lifetimes in the LMC are still notably underestimated in the 1.8−3.0 $M_\odot$ range.

Figure A.3 introduces a few important changes, namely (i) the assumption of constant λ is relaxed to account for a more realistic dependence on mass and metallicity according to K02 recipe; (ii) pulsation periods are calculated following the scheme indicated in Sect. 2.7, that predicts the mode switching from FOM ($P = P_1$) to FM ($P = P_0$); and (iii) the inclusion of an age-metallicity relation in the galaxy simulations instead of constant metallicity. As a matter of fact, the use of a $\lambda(M, Z)$ law significantly improves the results for the CSLF in the LMC, while a sizeable overproduction of luminous C stars affects the CSLF in the SMC. Moreover, the problem with the overly short M-star lifetimes still remains.

The way out of this latter discrepancy is obtained when we adopt the $M_{\rm c}^{\rm min}(M, Z)$ formalism suggested by K02, in place of the temperature parameter $T_{\rm b}^{\rm dred}$ to determine the onset of the third dredge-up. This effect is illustrated in Fig. A.4. The reason is that, while the $T_{\rm b}^{\rm dred}$ criterion predicts that models with $M_{\rm i} \gtrsim 2\ M_\odot$ experience the mixing events already from the first thermal pulse, with the $M_{\rm c}^{\rm min}(M, Z)$ scheme the onset of the dredge-up is delayed, then allowing for a longer duration of the M-type phase for these models.

We should also note that the theoretical CSLFs obtained with Z = const. notably differ from the observed ones in both Magellanic Clouds. The results gets better when assuming a proper AMR for the host galaxy, but the comparison with the observed data is still not completely satisfactory.

Finally, the best fit to the CSLFs, the M-type, and the C-type lifetimes in the Magellanic Clouds is reached with the aid of the scheme for the third dredge-up presented in Sect. 2.5. The original K02 formalism is partly modified in order to (i) correct for convective overshooting, (ii) anticipate the occurrence of the third dredge-up, (iii) and make it more efficient at lower metallicities. The results are displayed in Fig. 27.

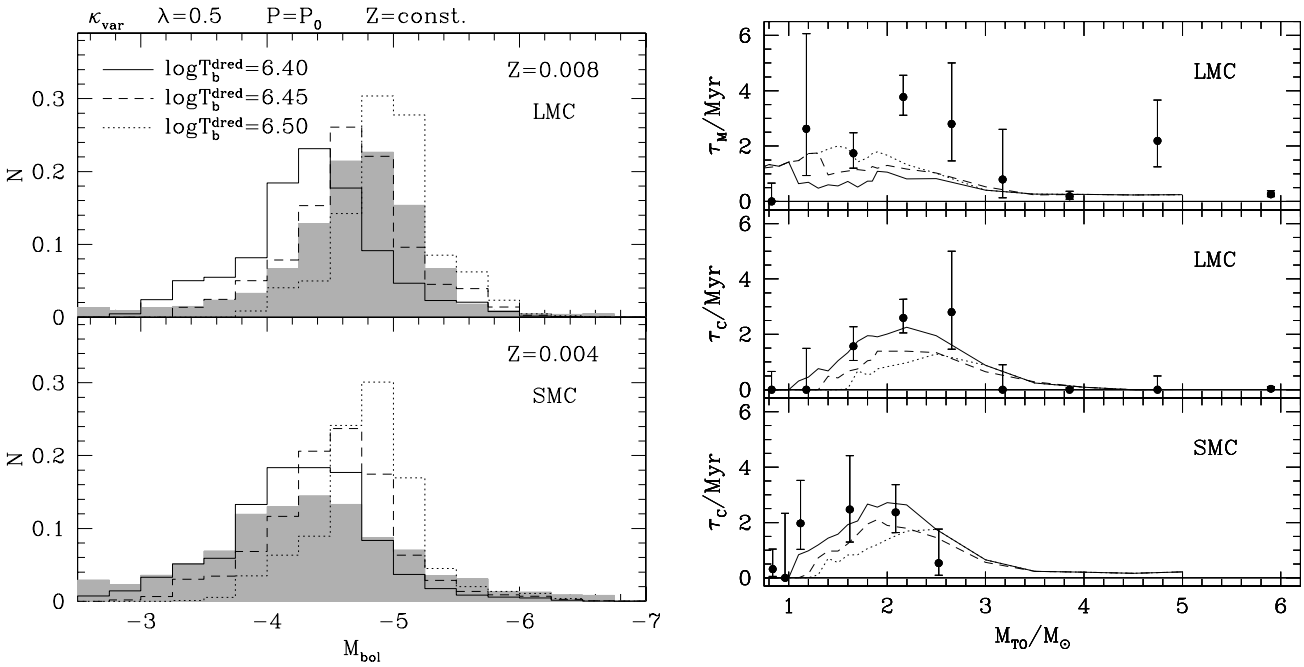

Fig. A.1. *Left panels*: The observed C star luminosity functions (CSLF) in the Magellanic Clouds (Groenewegen 2002; shaded areas), as compared to the synthetic ones derived from models with different dredge-up parameters, assuming Vassiliadis & Wood's (1993) mass-loss prescription and pulsation on the FM. *Right panels*: The observed C- and M-type lifetimes in the Magellanic Clouds (Girardi & Marigo 2007), as compared to the same set of models.

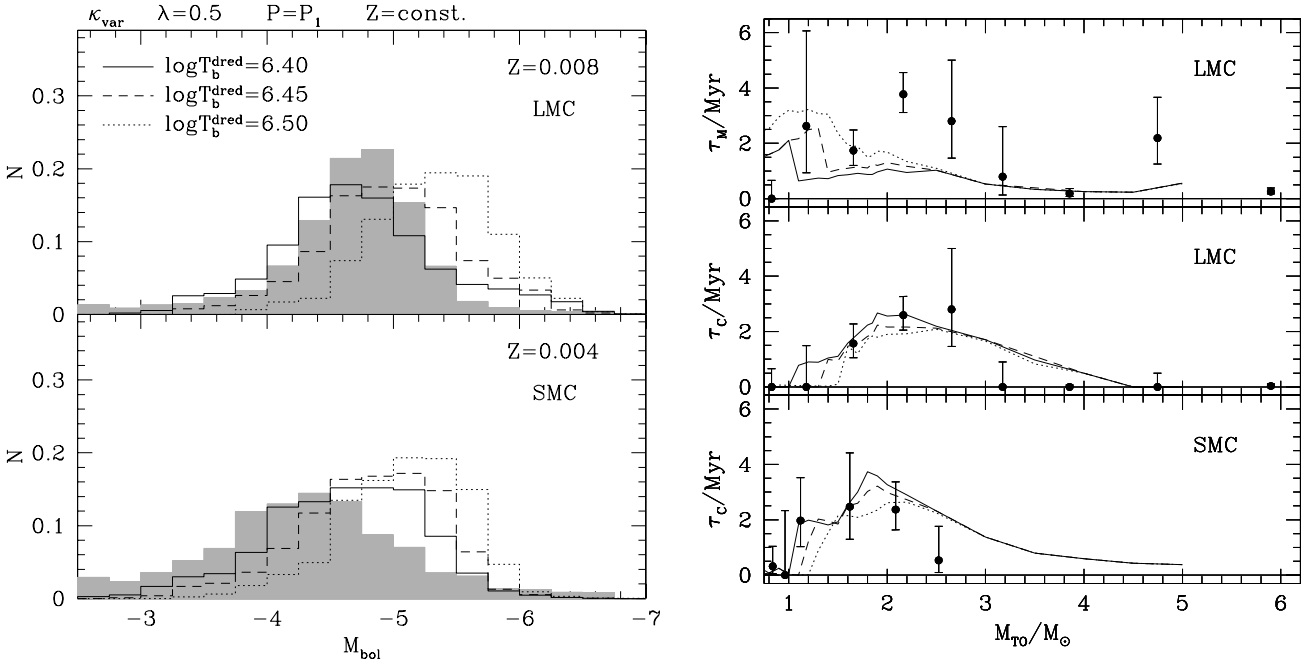

Fig. A.2. The same as Fig. A.1, but for models assuming pulsation on the FOM.

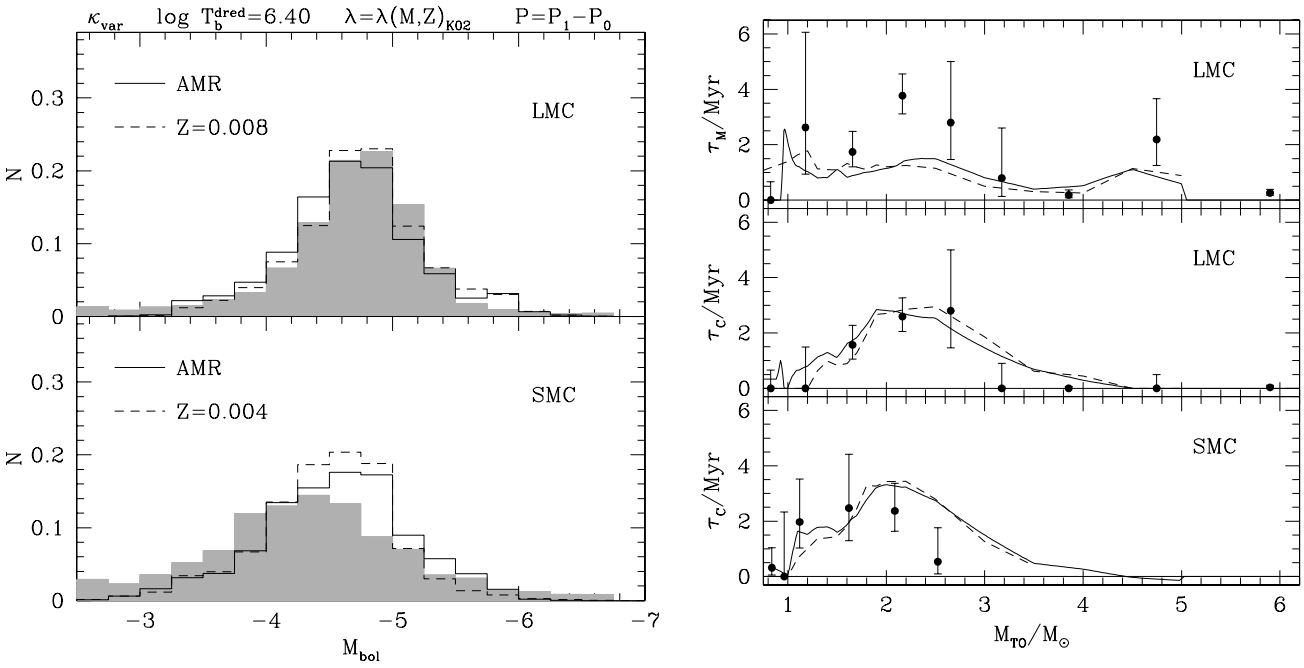

Fig. A.3. The same as Fig. A.1, but for models assuming a variable λ (K02), mode switching between FM and FOM, and an AMR. See the text for details.

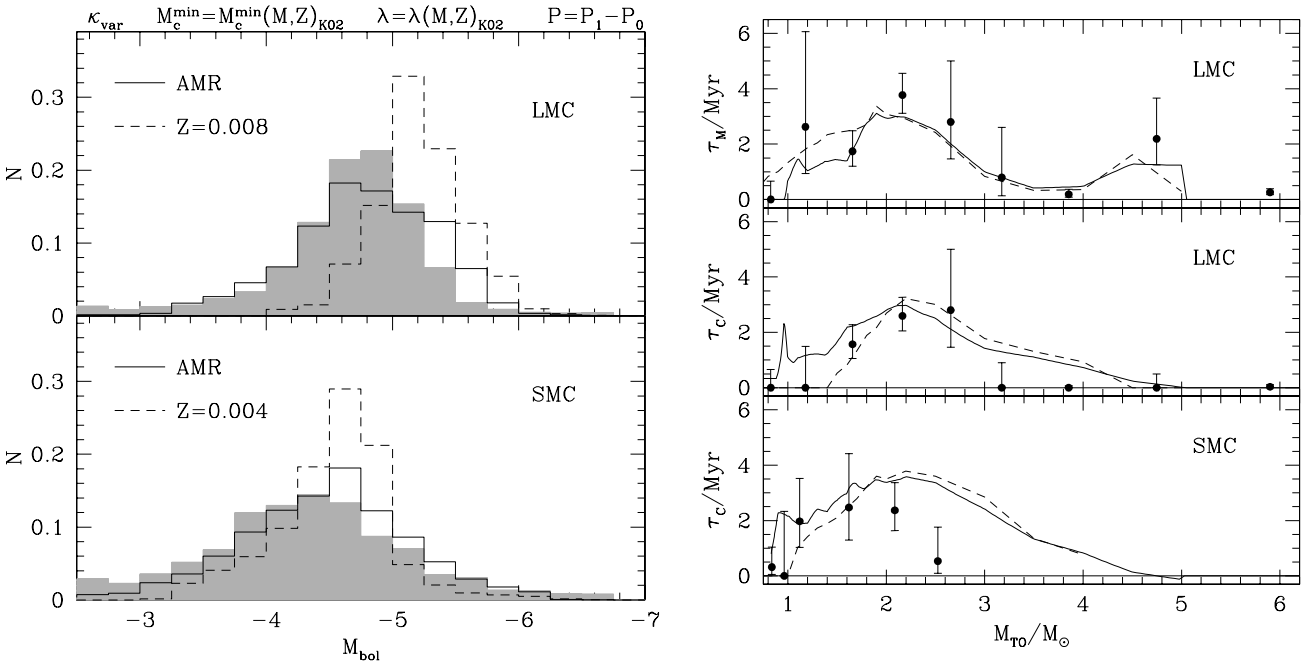

Fig. A.4. The same as Fig. A.3, but for models assuming the $M_{\rm c}^{\rm min}(M,Z)$ formalism suggested by K02.